Nearshore physical processes and bio-optical properties in the New York Bight

G. C. Chang,[1] T. D. Dickey,[1] O. M. Schofield,[2] A. D. Weidemann,[3] E. Boss,[4] W. S. Pegau,[4] M. A. Moline,[5] and S. M. Glenn[2]

Received 12 June 2001; revised 18 March 2002; accepted 2 April 2002; published 21 September 2002.

[1] Temporal and spatial variability of physical, biological, and optical properties on scales of minutes to months and meters to ~50 km are examined using an extensive data set collected on the New York Bight continental shelf during the Hyperspectral Coastal Ocean Dynamics Experiment. Measurements from a midshelf mooring and bottom tripod (~25 km offshore, 24 m water depth) and two nearshore profiling nodes (~5 km offshore, 15 m water depth) are utilized to quantify and correlate midshelf and nearshore variability. Towed shipboard undulating profilers and a high-frequency radar (CODAR) array provide complementary spatial data. We show that phytoplankton and dissolved matter each accounted for roughly 50% of total absorption (440 nm) at midshelf. In contrast, particulate compared to gelbstoff absorption dominated total absorption at the nearshore location. A relatively high-salinity, low-temperature, low particulate coastal jet decreased turbidity nearshore and advected lower-salinity, higher-chlorophyll waters to the midshelf region, resulting in increased biomass at midshelf. Small-scale (order of a few kilometers) convergence and divergence zones formed from the interaction of semidiurnal tides with mean currents and a water mass/turbidity front. The front resulted in increased decorrelation scales from nearshore (~1 day) toward midshelf (2–3 days) for optical and biological parameters. We conclude that optical and biological variability and distributions at midshelf and nearshore locations were influenced mainly by semidiurnal tides and the coastal jet. We present insights into nearshore coastal processes and their effects on biology and optics as well as for the design of future nearshore interdisciplinary coastal programs. *INDEX TERMS:* 4552 Oceanography: Physical: Ocean optics; 4546 Oceanography: Physical: Nearshore processes; 4528 Oceanography: Physical: Fronts and jets; 4223 Oceanography: General: Descriptive and regional oceanography; *KEYWORDS:* New York Bight, optics, physical/biological coupling, coastal jet, bio-optics

Citation: Chang, G. C., T. D. Dickey, O. M. Schofield, A. D. Weidemann, E. Boss, W. S. Pegau, M. A. Moline, and S. M. Glenn, Nearshore physical processes and bio-optical properties in the New York Bight, *J. Geophys. Res.*, *107*(C9), 3133, doi:10.1029/2001JC001018, 2002.

1. Introduction

[2] Over the past several decades, increasing numbers of oceanographic programs have shifted from open ocean studies to coastal ocean research. Improved understanding of coastal ocean physical processes and their effects on biology is necessary because the majority of the world's primary production occurs on continental shelves and physical processes in the coastal ocean are generally more dynamic and complex than in the open ocean. The surface area of the coastal zone ($\sim 26 \times 10^6$ km^2) is about 7% of the total surface area of the ocean ($\sim 360 \times 10^6$ km^2); total annual primary production in the coastal zone has been estimated to be 20% of total ocean production (6.0 Gt C yr^{-1} and 24 Gt C yr^{-1} in the coastal and open ocean, respectively) [*Wollast*, 1998]. Past studies in the North Atlantic indicate that coastal ocean summer productivity is almost twice as high as in areas directly offshore [*Mann and Lazier*, 1991]. Traditionally, coastal ocean research has been more focused on regions near the shelf break (e.g., Shelf Edge Exchange Processes I and II (SEEP-I and -II) [*Biscaye et al.*, 1988; *Biscaye*, 1994], Sediment Transport Events on Shelves and Slopes (STRESS) [*Trowbridge and Nowell*, 1994], and Coastal Mixing and Optics (CMO) [*Dickey and Williams*, 2001]), with few interdisciplinary field experiments within 25 km of the coast and in waters less than ~30 m. Oceanographic research within 25 km of shore is important because: 1) it is necessary to improve interdisciplinary models in the areas of high primary productivity to

[1]Ocean Physics Laboratory, University of California at Santa Barbara, Santa Barbara, California, USA.
[2]Institute of Marine and Coastal Sciences, Rutgers University, New Brunswick, N. J., USA.
[3]Naval Research Laboratory, Stennis Space Center, Miss., USA.
[4]College of Oceanic and Atmospheric Sciences, Oregon State University, Corvallis, Oregon, USA.
[5]Biological Sciences Department, California Polytechnic State University, San Luis Obispo, California, USA.

0148-0227/02/2001JC001018$09.00

quantify the global carbon budget, and 2) it is estimated that nearly 50% of the world's population lives within 1 km of the coastal ocean and anthropogenic effects of population expansion on the coastal ocean are poorly understood.

[3] Understanding the variability of physical, hydrographic, biological, and optical properties and the relationships between these properties is necessary for the design (e.g., determination of limits on grid spacing and time steps) of accurate coupled physical-biogeochemical models and for the interpretation of remote sensing data in the nearshore coastal ocean. Nearshore research is difficult because physical processes in this region are not only affected by shelf slope dynamics, but also by river and estuarine flow, bottom topography, and the shape of the coastline. Biological and optical variability is influenced by phytoplankton growth and grazing, exudation of dissolved organic matter, and several physical processes (advection by mean currents, upwelling, tides, waves, eddies, jets, meanders, etc.). Other processes such as geological processes (e.g., sediment resuspension and transport, flocculation and deflocculation), chemical photo-oxidation, and anthropogenic effects (sewage outflows, desalination plants, chemical dumping and burial, etc.) can also affect distributions of optical properties.

[4] The current study builds on previous experiments that investigated temporal and spatial variability of bio-optical properties as related to physical processes in the coastal ocean (e.g., CMO [*Chang*, 1999; *Chang and Dickey*, 2001] and open ocean sites [*Dickey et al.*, 1991, 1993, 1994, 1998a, 1998b, 2001]) using moorings and tripods, drifters (e.g., Coastal Transition Zone (CTZ) program in the California Current [*Abbott et al.*, 1995; *Abbott and Letelier*, 1998]), and shipboard transects (e.g., Marine Light-Mixed Layers (MLML) program using profile and tow-yo data [*Washburn et al.*, 1998] and SeaSoar data in the Arabian Sea [*Lee et al.*, 2000]). Physical processes found important to bio-optical variability in the Middle Atlantic Bight (MAB) during the CMO program include, but are not limited to: storms and hurricanes, shelf slope frontal movement, Gulf Stream eddies, meanders, filaments, jets, tides, and internal solitary waves (ISWs) [*Chang*, 1999; *Chang and Dickey*, 2001]. Results from the CTZ program showed that large-scale spatial and temporal variability of bio-optical and biological properties was influenced by changes in phytoplankton species composition. These shifts in phytoplankton community structure were found to be associated with the meandering circulation of the California Current. Further, fluctuations of bio-optical properties were found on diel, semidiurnal, and inertial temporal scales, which were attributed to solar variations and internal tides [*Abbott et al.*, 1995]. *Washburn et al.* [1998] examined water mass variability and phytoplankton distributions in a mesoscale eddy field in the North Atlantic open ocean. They concluded that eddy advection controlled phytoplankton distributions. The Arabian Sea results demonstrate that chlorophyll fluorescence varied at smaller scales than hydrographic properties, indicating that biology was influenced not only by physical processes, but also biological control, e.g., interactions between phytoplankton growth and zooplankton grazing [*Lee et al.*, 2000]. *Lee et al.* [2000] also show that diel variability may be important to phytoplankton decorrelation scales. The programs described above differ from the present study in that their field experiments were conducted in deeper waters at the shelf break and beyond.

[5] *Mountain* [1991] describes the hydrography of the MAB shelf waters as being relatively low in temperature and salinity in comparison to the slope water found farther offshore, with salinity values typically less than 34.0 psu. It has been determined that the shelf waters of the MAB and the New York Bight (NYB) originate from the Gulf of Maine, the Scotian Shelf, the MAB continental slope, and local river input [*Mountain*, 1991]. Waters from the Gulf of Maine and the Scotian Shelf are mixed and modified by local processes (seasonal heating, cooling, precipitation, and evaporation) within the Gulf of Maine, then transported to the MAB over Georges Bank, southwestward around Cape Cod, and south toward Cape Hatteras (Figure 1). Water is advected off of the shelf along the shelf slope front and at Cape Hatteras.

[6] Shelf break eddies, jets, and meanders, and Gulf Stream rings have been observed to mix higher-salinity slope waters with MAB shelf waters near the shelf break throughout the year [e.g., *Pickart et al.*, 1999; *Chang and Dickey*, 2001]). *Brooks* [1996] reported that persistent southward coastal jets extending approximately 5–10 km offshore often form along the east coast of the U.S. These jets are characteristic of flow reversals in response to the relaxation of upwelling favorable winds (R. J. Chant et al., manuscript in preparation, 2002). The flow reversals have been observed in coastal upwelling regions of New Jersey, Oregon, and California [*Chelten et al.*, 1988; *Barth et al.*, 1999]. R. J. Chant et al. (manuscript in preparation, 2002) show that during the onset of upwelling favorable winds, subsurface onshore transport often does not compensate for the surface offshore transport. In response, the nearshore jet forms over an inertial period during maximum alongshelf wind stress in the vicinity of an upwelling center. The surface offshore transport then exceeds the Ekman transport, suggesting that the offshore transport is augmented by an alongshore convergence of the nearshore jet. These jets, coupled with weak counterclockwise eddies that are often observed during the summer and through the late fall, result in relatively short residence times (6 to 10 days) for water parcels in the NYB [*Bumpus*, 1973].

[7] The maximum energy in the water column has been found to be near the semidiurnal tidal frequency, with less importance from the diurnal tidal frequency, particularly in the stratified spring and summer months [*Mayer*, 1982; *Flagg et al.*, 1994; *Chang and Dickey*, 2001]. Local river runoff is generally more significant on the inner continental shelf. Over the entire MAB, the river runoff is almost two orders of magnitude smaller than the water mass contributions from the Gulf of Maine and the Scotian Shelf [*Mountain*, 1991].

[8] Physical processes (e.g., storms and hurricanes, shelf slope frontal movement, eddies, tides, river and estuarine inputs, etc.) promote high-nutrient fluxes onto the relatively shallow shelf waters of the MAB and result in extremely high rates of primary productivity compared to much of the rest of the world's oceans [*Bourne and Yentsch*, 1987; *Mann and Lazier*, 1991; *Wollast*, 1998]. Cross-shelf advective inputs of nutrients during spring and summer upwelling winds also lead to increased primary productivity in the NYB [*Sherman et al.*, 1996]. The highest estimated primary production between New Jersey and North Carolina has been reported to be 505 gC m^{-2} yr^{-1} [*Sherman et al.*, 1996].

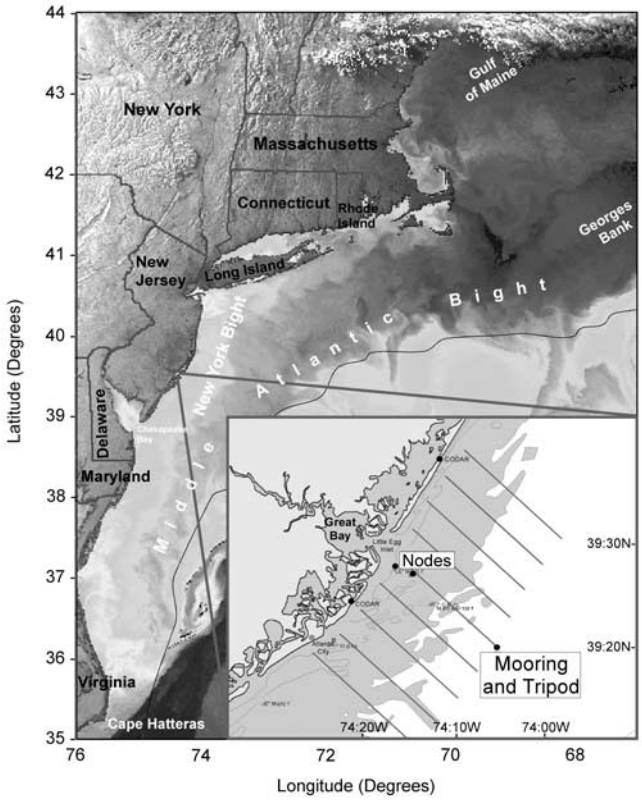

Figure 1. Advanced very high resolution radiometer (AVHRR) sea surface temperature map of the Middle Atlantic Bight and the New York Bight obtained on June 10, 2000. The black line denotes the approximate location of the shelf slope front. Inset: site map of the spring and summer 2000 HyCODE field experiment. Black dots specify the approximate locations of the midshelf mooring and tripod, the nearshore profiling nodes, and the CODAR antennae. Lines extending offshore indicate ship tracks.

SEEP-II findings indicate that approximately half of primary production is consumed on the MAB continental shelf during the spring bloom [*Biscaye et al.*, 1994; *Kemp*, 1994]. Also, a large fraction of biological material sinks to the seafloor and is degraded by benthic microbial activity in the nepheloid and benthic layers [*Kemp*, 1994]. Up to 25% of the spring production is estimated to be available for export to the continental slope or the deep ocean [*Kemp*, 1994].

[9] The present study is part of the Office of Naval Research (ONR) sponsored Hyperspectral Coastal Ocean Dynamics Experiment (HyCODE). One site of the HyCODE experiment is the Long-Term Ecosystem Observatory (LEO-15) on the New Jersey shelf of the New York Bight (NYB) in the MAB in less than 25 m water depth (Figure 1). One of the central goals of the program is to determine how temporal and spatial variability in inherent optical properties (IOPs) is affected by the dynamical physical processes in the shallow (<25 m water depth), coastal ocean, within 25 km of shore. The approach is to use complementary sampling methods (e.g., shipboard measurements, moorings, tripods, autonomous underwater vehicles (AUVs), underwater profiling nodes, high-frequency radar (CODAR), and hyperspectral imagery) to investigate temporal and spatial variability of physical processes that affect variability of optical and biological parameters on scales of minutes to seasons and meters to ~50 km. These include the range of scales associated with tides, internal gravity waves, storms, upwelling and frontal activity, mesoscale events, estuarine flows, phytoplankton community-scale adaptations, and phytoplankton light and nutrient adaptations. We hypothesize that variability and distributions of bio-optical properties are controlled by physical processes, mainly advection and tides that occur on the NYB inner continental shelf. We also hypothesize that the processes governing the optical and biological properties differ between nearshore (within ~5 km of shore and waters shallower than 15 m; highly turbid) and midshelf (~25 km offshore) locations, with decorrelation scales increasing from nearshore to midshelf. Also, we believe that spatial scales are influenced by relatively small-scale (on the order of a few kilometers or less) convergence and divergence zones.

2. Methods

[10] Several instruments were deployed on the midshelf mooring and the bottom tripod during the HyCODE field experiment between May 16 and September 15, 2000, at about 39°20′N, 74°05′W in 24 m water depth (~25 km offshore) to concurrently collect high temporal resolution physical and bio-optical measurements at several depths (Figures 1 and 2). Most of the instruments were recovered and redeployed on July 25, 2000. Physical and bio-optical instruments included: temperature sensors (Onset Computer Corp. Tidbits and Sea-Bird, Inc. Seacats, Microcats, and

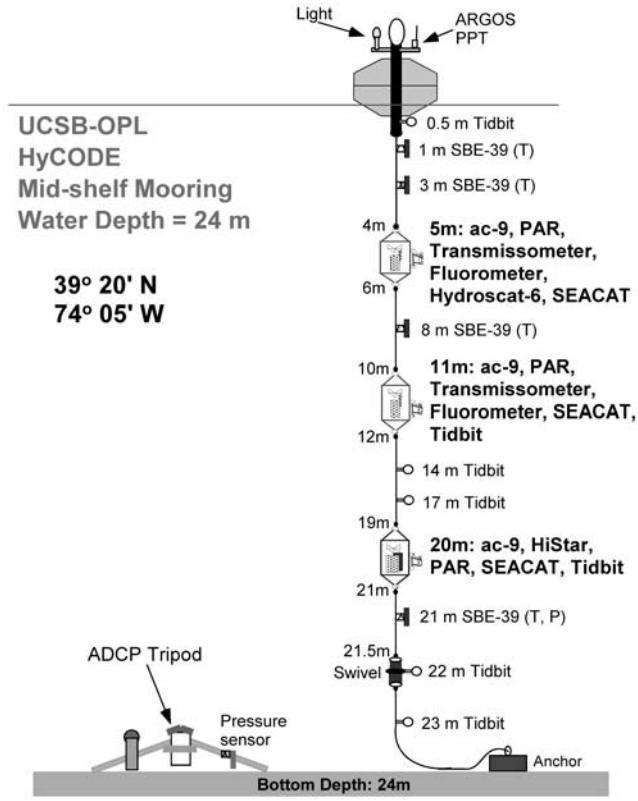

Figure 2. Schematic diagram of midshelf mooring and tripod.

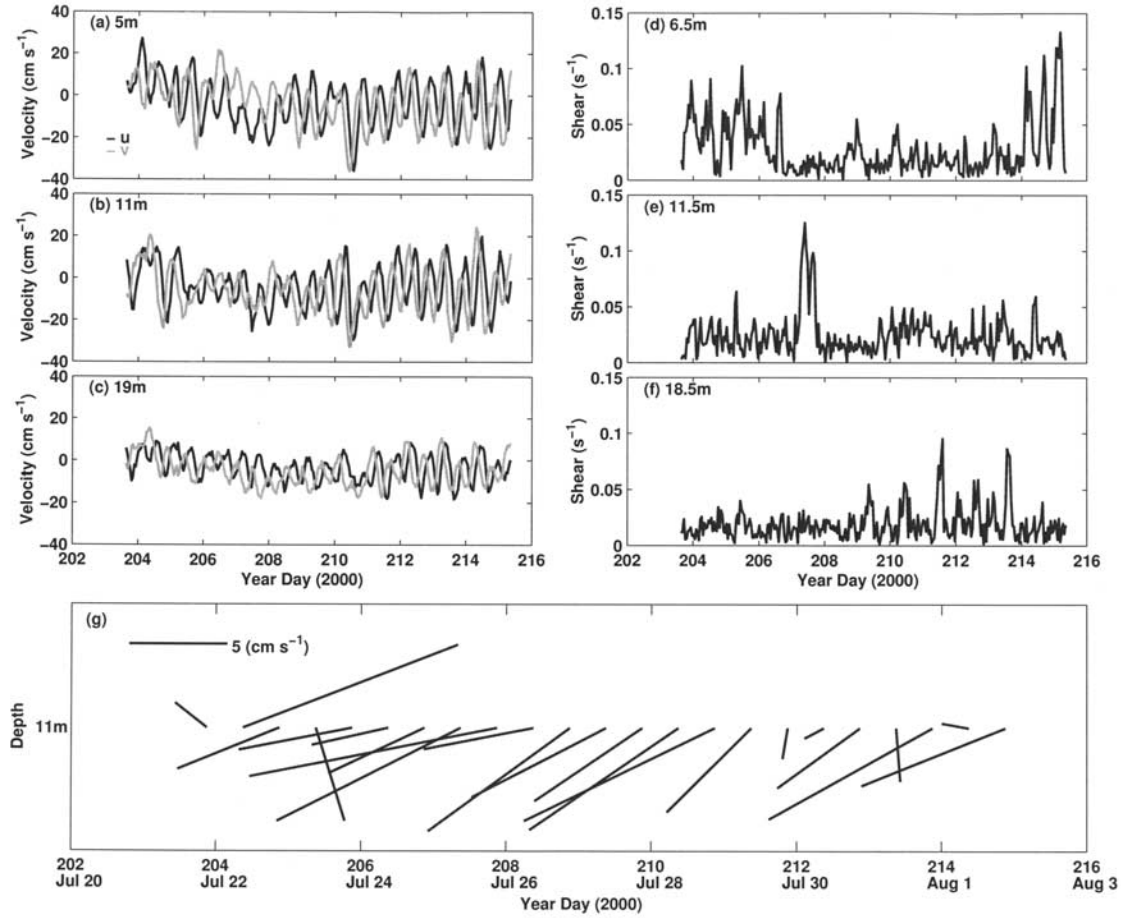

Figure 3. Time series of east (u) and north (v) component current velocity at (a) 5 m, (b) 11 m, and (c) 19 m; shear calculated at (d) 6.5 m, (e) 11.5 m, and (f) 18.5 m (Δz used for shear calculations was 1 m); (g) stickplots of detided currents at 11 m water depth (5 cm s^{-1} scale bar is located in the top left corner), all obtained from the midshelf bottom-mounted ADCP.

SBE-39s) at about every 3 m between 1 and 24 m; salinity sensors (Seacats and Microcats), spectral absorption-attenuation meters (WET Labs, Inc. ac-9s; wavelengths are: 412, 440, 488, 510, 532, 555, 650, 676, and 715 nm) at 5, 11, and 20 m; fast sampling WET Labs, Inc. beam transmissometers (660 nm; C-Stars) and fluorometers (WETStars) at 5 and 11 m; a backscattering instrument (HOBI Labs HydroScat-6; wavelengths are 442, 470, 510, 589, 620, and 671 nm [*Maffione and Dana*, 1997]) at 5 m; and an RD Instruments uplooking acoustic Doppler current profiler (ADCP) on the bottom tripod at 24 m. The sampling rates of the temperature sensors ranged from one to five minutes. The fast sampling transmissometers and fluorometers sampled at 10 Hz for a four second period every minute, and the sampling rate for the ac-9 and Hydroscat-6 (1 Hz) was once per hour and once every two hours, respectively. For more details regarding mooring and tripod instrumentation, see *Chang et al.* [2000], *Dickey et al.* [2000], and http://www.opl.ucsb.edu/hycodeopl.html.

[11] Vertical profiles of physical and bio-optical instruments were made from two underwater nodes (a CTD node and an optical node) about 12 m apart, located at 39°27.42′N, 74°14.75′W in approximately 15 m water depth (~5 km offshore; Figure 1). Each node is a moored platform connected to various instruments by an electro-optic cable that provides real-time data and power. A mechanical winch releases the cable during profiling, allowing a positively buoyant instrument package to ascend to the surface. Profiles of temperature, salinity, chlorophyll fluorescence, and optical backscatter were taken every hour between July 21 and August 3, 2000, using the CTD node. Profiles of optical properties using an ac-9 were collected every half hour from July 19 until August 3, 2000, using the optical node. The ascent/descent rates were ~2.5 and 3 m min^{-1} for the optical and CTD nodes, respectively. Both upcasts and downcasts were utilized for analyses.

[12] Intensive shipboard sampling was conducted from July 7 to August 3, 2000, along eight cross-shelf transects off the New Jersey coast extending 25 km offshore and 20 km to the north and south of Great Bay (Figure 1). A package equipped with FSI temperature and salinity sensors, a WET Labs, Inc. fluorometer, and an optical backscattering instrument (single wavelength) was towed using an undulating guildline towbody behind the R/V *Caleta*. Tow-yo transects were performed nearly daily from July 7 to August 3, 2000 (see http://marine.rutgers.edu/cool/hycode/data/calendar.html for detailed ship schedule information). Profiles of IOPs at midshelf and nearshore were

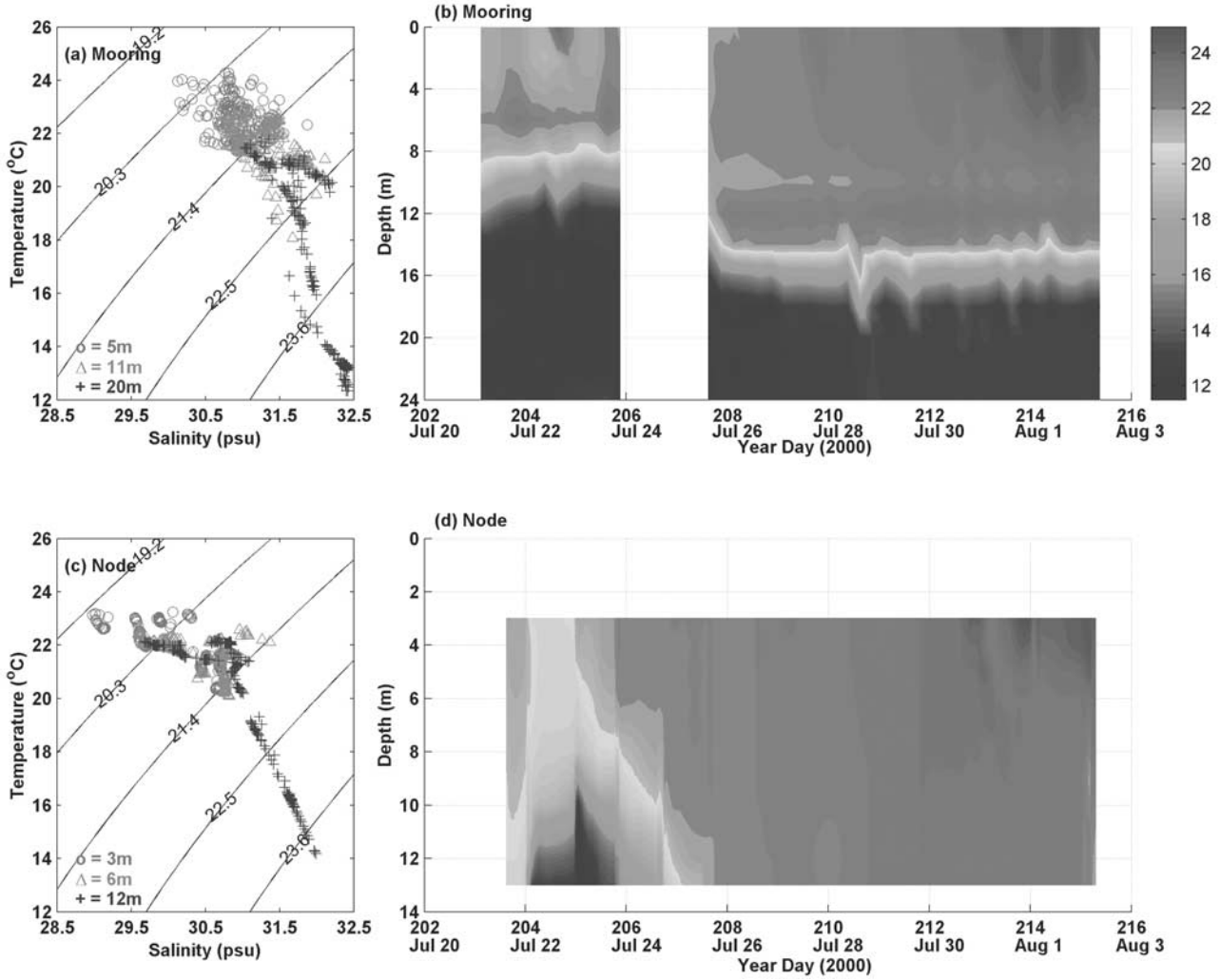

Figure 4. (a) The 4 hour averaged temperature versus salinity (T-S) data, and (b) the time series contour plot of the 4 hour averaged temperature from the midshelf mooring (the temporal gap is when mooring instruments were recovered and redeployed); (c) the 1 hour averaged temperature versus salinity data, and (d) the time series contour plot of the 1 hour averaged temperature from the nearshore profiling node. Density lines on T-S plots were calculated according to *United Nations Educational, Scientific, and Cultural Organization* (*UNESCO*) [1981] algorithms and are labeled. The color scale bar represents Figures 4b and 4d. See color version of this figure at back of this issue.

collected by use of the slow descent rate optics platform (Slowdrop) from the R/V *Northstar*. Instruments on Slowdrop include two spectral absorption attenuation meters (ac-9s; wavelengths are listed above), a CTD, and a fluorometer. To determine the contribution of colored dissolved materials to the total absorption coefficient, a 0.2 μm filter (Gelman Suporcap 100) was attached to the inlet of one of the ac-9s. Both instruments were calibrated daily with optically pure water as a reference (Barnstead NANOpure).

[13] Surface current fields were mapped using a medium-range CODAR array covering approximately 1600 km^2 of the coastal ocean off of Great Bay, New Jersey. Surface current horizontal spatial resolution was ~1 km. The range of CODAR extended about 40 km offshore. Data were collected once per hour on the hour over the period of the summer 2000 HyCODE field experiment.

[14] Temperature, salinity, chlorophyll fluorescence, absorption, and attenuation from the mooring and nodes and data from the midshelf tripod ADCP during the time period of July 21 to August 3, 2000, are presented in this manuscript. Temperature, salinity, and chlorophyll fluorescence data collected during tow-yos between July 21 and August 1, 2000, along (A line), just north (N1 line), and just south (S1 line) of the cross-shelf transect line directly offshore from Little Egg Inlet of Great Bay are shown. Data from nine transects are utilized. Slowdrop profiles of absorption (dissolved and particulate) and chlorophyll fluorescence data from near the midshelf mooring and the nearshore node are shown here as well. Chlorophyll *a* was derived from the mooring fluorometers following the methods presented by *Chang* [1999]. Chlorophyll fluorescence data from the R/V *Caleta* and the node are an indicator of phytoplankton biomass and reported in relative fluorescence units (RFU).

[15] Optical properties collected during HyCODE are utilized to distinguish between biological, detrital (defined

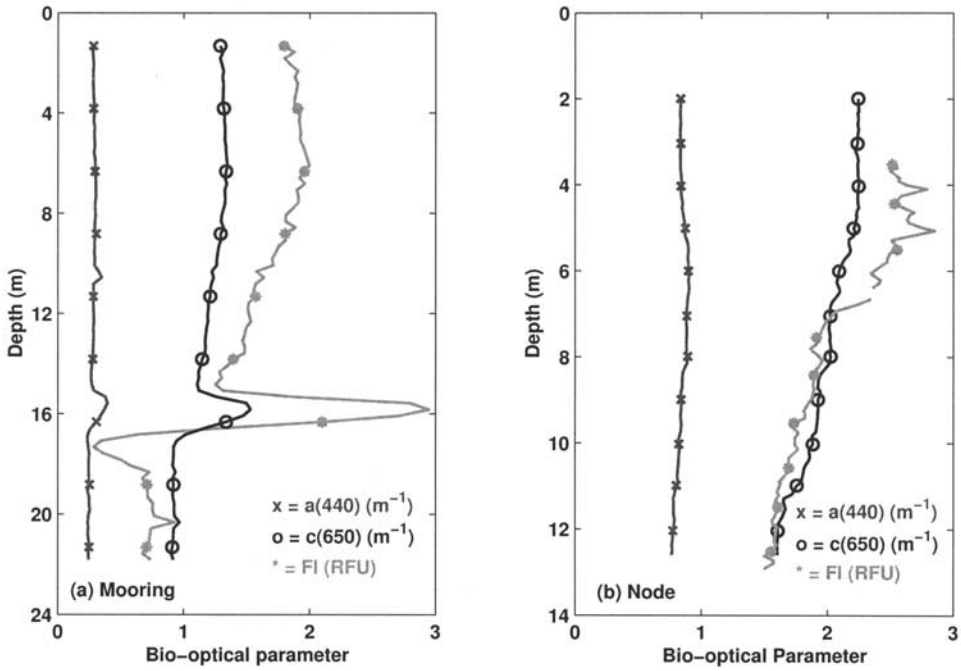

Figure 5. Profiles of $a_{t-w}(440)$ and c(650) (both in m^{-1}) from the ac-9 and chlorophyll fluorescence (in relative fluorescence units, RFU) taken on July 26, 2000 (a) at the midshelf mooring and (b) at the nearshore node; time series of (c) chlorophyll *a* (derived from fluorometers) at 5 and 11 m, (d) $a_{t-w}(440)$, and (e) c(650) at 5, 11, and 20 m from the midshelf mooring; time series of (f) chlorophyll fluorescence (RFU), (g) $a_{t-w}(440)$, and (h) c(650) at 3, 6, and 12 m from the nearshore node. The gap in chlorophyll fluorescence time series seen from July 27 to 29 was due to servicing of the CTD node (cleaning of the optical windows).

as all nonchlorophyll containing particles of organic or inorganic origin), and dissolved matter. Phytoplankton is inferred from the chlorophyll *a* absorption peak in particulate absorption at 440 nm, or from total minus water absorption at 676 nm ($a_p(440)$ or $a_{t-w}(676)$, respectively). Gelbstoff absorption in the blue wavelengths (412 nm or 440 nm, $a_g(412)$ or $a_g(440)$, respectively) serves as a proxy for dissolved matter. Lastly, beam attenuation at 650 nm (c(650)) and optical backscatter are used as a measure of turbidity (defined as water clarity influenced by particles) in the water column. Profiled gelbstoff absorption ($a_g(\lambda)$) and total minus water absorption ($a_{t-w}(\lambda)$) data were utilized to quantify the influence of particulates ($a_p(\lambda)$, by difference) and colored dissolved matter on total absorption. Scatterplots of chlorophyll *a* (derived from the fluorometers or absorption in the near infrared wavelengths; see *Chang* [1999]; chlorophyll fluorescence presented for node data) versus turbidity (c(650) or optical backscatter) at near surface (5 and 3 m at mooring and node, respectively), intermediate (11 and 6 m), and near bottom (20 and 12 m) depths were used to qualitatively differentiate the phytoplankton from detrital particles [*Wu et al.*, 1994; *Chang*, 1999; *Chang et al.*, 2001]. High chlorophyll *a* (fluorescence) values with relatively low-beam c (turbidity) are indicative of phytoplankton, whereas high beam c (turbidity) values with relatively low-chlorophyll *a* (fluorescence) values imply detrital material. Qualitative partitioning of particle type was also done by utilizing scatterplots of the ratio of backscattering to total scattering coefficient at ~440 nm ($b_b(442)/b(440)$) versus the ratio of chlorophyll *a* to beam c (Chl *a*/c(660)) at 5 m at midshelf only (following *Boss et al.* [2001]).

[16] Statistical analyses of temporal and spatial variability are utilized. Frequency autospectra were computed in order to quantify the temporal variability of the physical, hydrographic, optical, and biological data. The autospectra were calculated using 192-point fast Fourier transforms (FFTs) tapered with a Hanning window, zero overlap, and $N \cong 300$ points for 1 hour averaged time series mooring data at all available depths and node data at 3, 6, and 12 m depths. Node depths were chosen to correlate with relative depths of the mooring instruments (e.g., 5 m at the mooring represented ~1/5 of the water column, therefore, in 15 m water depth at the node, 3 m was chosen because it was ~1/5 of the water column). Timescale autocovariances were computed for temperature, salinity, density, chlorophyll fluorescence, beam c, and absorption (440 nm) data at all available mooring depths and at 3, 6, and 12 m for the nodes to determine the timescales of decorrelation of the various physical and bio-optical properties. Data were not averaged for the autocovariance analyses. Autocovariances for data from nine ship transects were computed for temperature, salinity, density, and chlorophyll fluorescence data averaged within the mixed layer. Coherence and associated phase functions were used to quantify the relationships between two variables at a range of frequencies, for specified phase lags. Coherence and phase estimates were made between chlorophyll fluorescence and various hydrographic properties to investigate the impact of water masses on phytoplankton. Coherences between absorption at 440 and 676

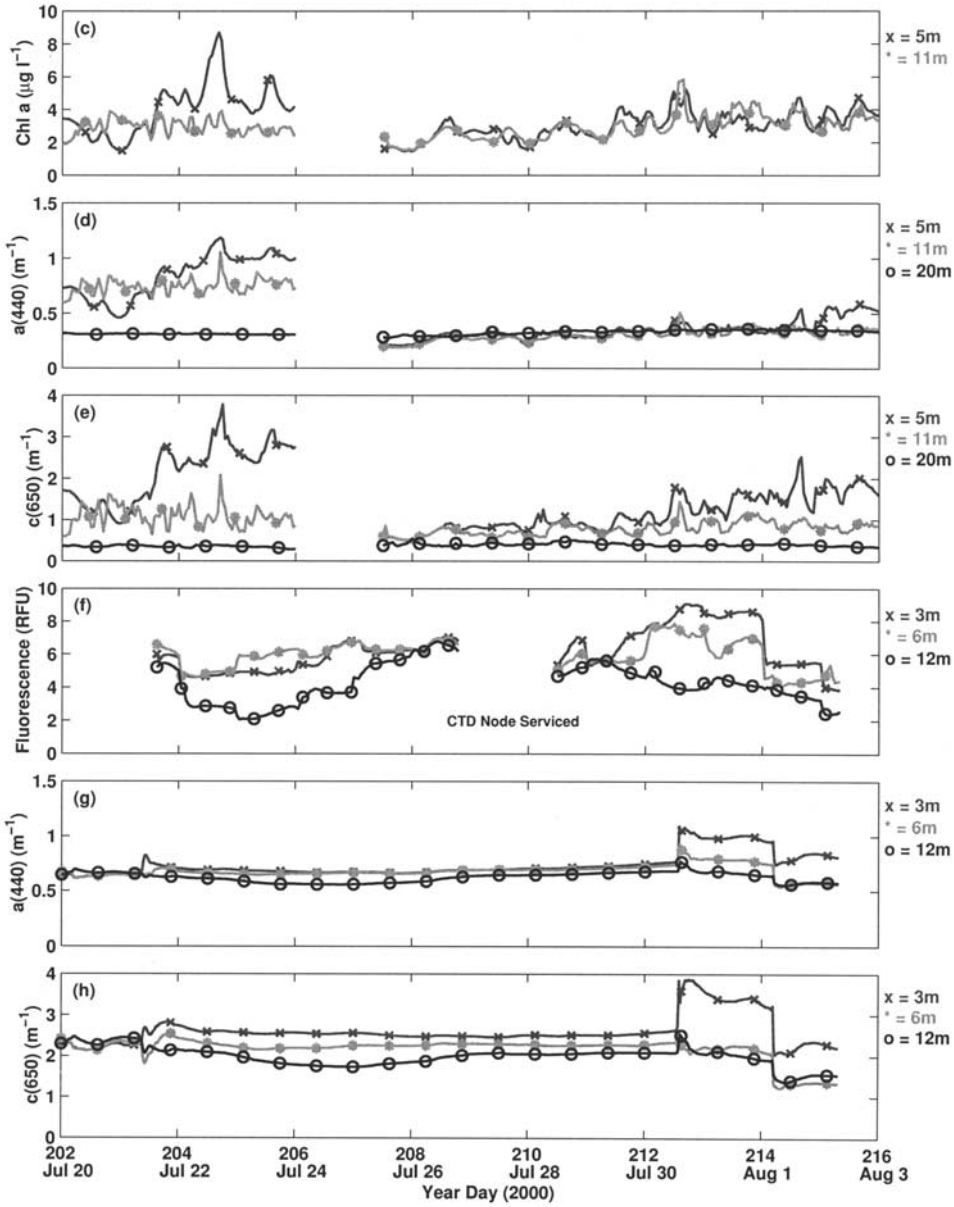

Figure 5. (continued)

nm and hydrographic properties were calculated to quantify the effects of water masses on phytoplankton variability. Lastly, coherence between attenuation at 650 nm and temperature and salinity were computed to examine the influence of water masses on turbidity in the water column. Coherence functions and phase were calculated using 64 point FFTs for N $\cong$ 200 data points for $\sim$10 degrees of freedom. Time series were tapered with Hanning windows, with 0 point overlaps and removal of means. Frequencies were converted to periods in days. Statistical significance levels were calculated according to *Thompson* [1979].

3. Results

3.1. Circulation

[17] The mean current transport direction at the HyCODE site was generally toward the southwest (alongshelf; Figures 1 and 3), although eddy-like turning of the currents can be seen sporadically throughout the entire midshelf mooring current time series (May 16 to September 15, 2000; not shown) as well as in surface CODAR images (data not shown). Minimum and maximum current speeds between July 21 and August 3, 2000, were 1.0 and 43.7 cm s^{-1}, respectively at 5 m depth; average current speed was 15.1 cm s^{-1}. Current shear was variable between depths, with values generally below 0.05 s^{-1}, but sometimes peaking close to 0.15 s^{-1} (Figure 3). Tides were generally barotropic over the time period of July 21 to August 3, 2000.

3.2. Hydrography

[18] Temperature versus salinity (T-S) diagrams from the nearshore node and midshelf mooring at the HyCODE site indicate that temperature and salinity ranged between 12 and 26°C and 28.5 and 32.5 psu, respectively (Figure 4). As expected, salinity at the nearshore node, close to the mouth of Great Bay, NJ, is lower than at midshelf. The water

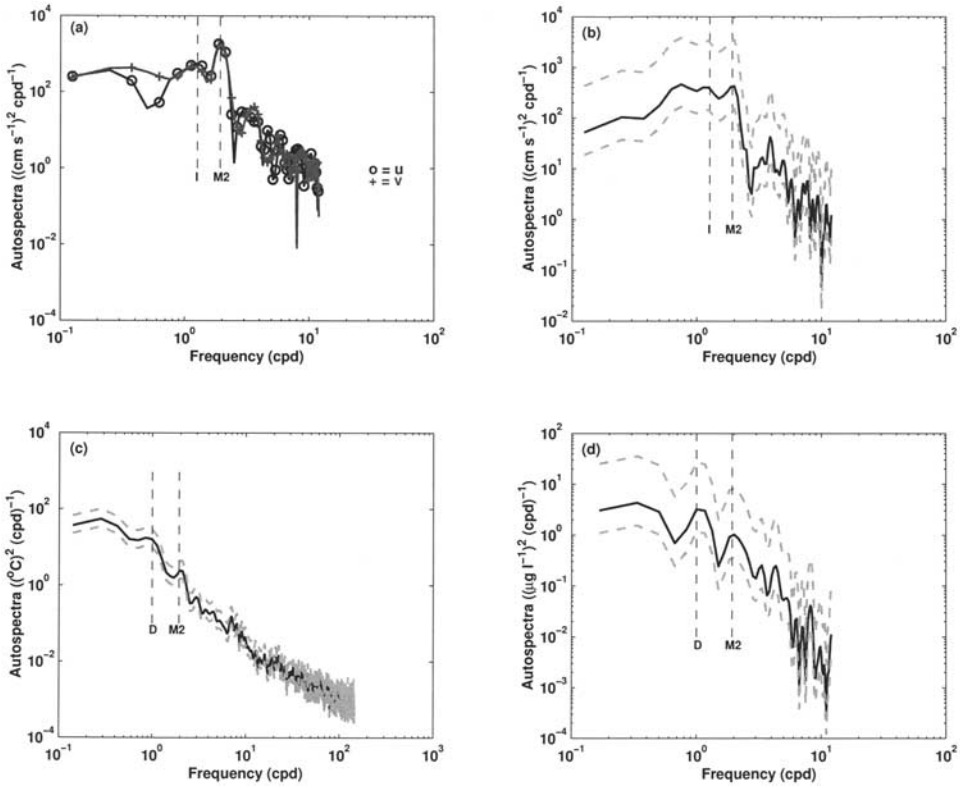

Figure 6. Frequency autospectra calculated for (a) 5 m east and north component current velocity, (b) 5 m current speed, (c) 0.5 m temperature, and (d) 5 m chlorophyll *a*, all at the midshelf mooring. Dashed lines signify 95% confidence intervals for Figures 6b, 6c, and 6d. Vertical lines indicate semidiurnal tidal (M2), inertial (I), and diel (D) frequencies and are labeled.

column was stratified between July 21 and August 3, 2000, at the midshelf location (Figure 4). Mixed layer depth (MLD; calculated using a 1° temperature criterion) was ~8 m, increased to ~14 m on July 26, then shoaled to ~5 m on August 1. A similar pattern was found in the time series of MLD at the nearshore location (MLD increased from ~8 m to almost the entire water column, then shoaled to ~4 m).

3.3. Optics and Biology

[19] Optical and biological properties at the midshelf mooring were generally nearly uniform from near the surface to the MLD and from just below the MLD to near the bottom. A distinct chlorophyll *a* maximum (also seen in a(440), and c(650)) was observed just below the MLD (Figure 5). A bottom nepheloid layer is not visible in the optical and biological profile data; instruments were positioned about 1.5 m above the seafloor. Note that mooring instruments were recovered and redeployed between July 24 and July 25, 2000.

[20] Nearshore optical and biological variability differed from that at the midshelf. Absorption (440 nm) and attenuation (650 nm) were more uniform throughout the water column and values were higher compared to those at the midshelf mooring (Figure 5; July 26 shown; note different depth scales between Figures 5a and 5b) Although not present in Figure 5, a bottom nepheloid layer starting at ~11 m depth is sometimes seen in the profiled bio-optical data from the nearshore node, particularly after July 30. A distinct chlorophyll fluorescence maximum was absent from profiled node data (Figure 5c; July 26 shown). Absorption, attenuation, and chlorophyll fluorescence were generally higher near the surface, decreasing at ~7 m water depth (1% and 10% light level was 10.0 and 5.3 m, respectively; data not shown). The gap in chlorophyll fluorescence data on July 27 is due to servicing of the node (optical windows were cleaned; Figure 5f).

3.4. Scales of Temporal Variability

[21] Frequency autospectra (see Methods section) of physical, hydrographic, optical, and biological properties at the midshelf mooring indicate that the dominant frequency in temporal variability of all properties at all depths was at the M2 semidiurnal tidal period. Tides were especially important for the currents (Figure 6). The inertial signal (~19 hours) was present only in the current velocity autospectra. The O1 diurnal tidal period (~25.82 hours) was not important to the temporal variability of physical, optical, and biological properties. As expected, near surface temperature and MLD autospectra exhibited a strong peak at the diel frequency due to daytime warming and nighttime cooling of the upper water column (Figure 6). The diel period was important for variability of chlorophyll *a* and absorption at 440 and 676 nm, in addition to absorption at each wavelength relative to 676 nm (Figure 6; chlorophyll *a* shown). Diel variability of optical and biological properties was likely due to changes in concentration of plankton because of MLD variability; however, several other processes can also contribute to diel cycling [e.g., *Hamilton et al.*, 1990; *Stramska and Dickey*, 1992, 1998]. Attenuation did not exhibit the diel variability,

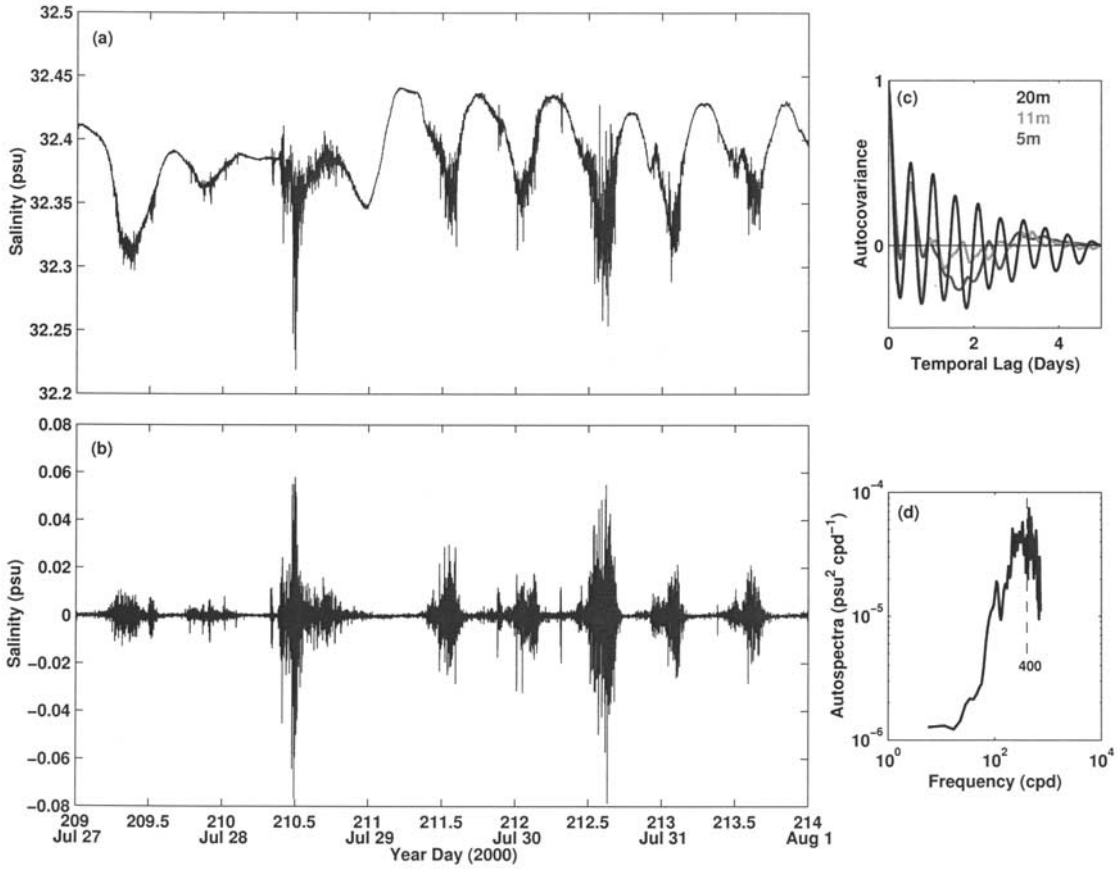

Figure 7. Time series of (a) 20 m salinity and (b) high-pass filtered (3 min) salinity recorded at 20 m; (c) autocovariance of salinity at 5, 11, and 20 m; and (d) frequency autospectra of high-pass filtered salinity at 20 m, all from the midshelf mooring between July 27 and August 1, 2000, illustrating the passage of internal solitary waves (ISWs).

except near the surface where the influence of the MLD is strongest (not shown). High-frequency variability (>5 cycles day^{-1}) was prominent in all physical, hydrographic, optical, and biological properties at all depths as well.

[22] Nearshore node frequency statistics were similar to those at the midshelf. The diel signal was important in near surface temperature, MLD, chlorophyll fluorescence, absorption, and attenuation due to daytime warming and nighttime cooling of the upper water column (data not shown). The dominant signal in physical, hydrographic, optical, and biological properties at all depths was at the M2 semidiurnal tidal period, although peaks in the autospectra were not as large as those found at the midshelf mooring (Figure 6; midshelf mooring data shown). The inertial and O1 diurnal tidal periods were not important for nearshore variability. Peaks at high frequency were present but also not as pronounced as for midshelf mooring autospectra. Slopes in nearshore autospectra were steeper than those found at the midshelf location. These differences can be attributed to higher turbulence in the shallower waters at the nearshore node.

3.5. Internal Solitary Waves (ISWs)

[23] Passages of internal solitary waves (ISWs) past our mooring were observed between July 27 and August 1, 2000 (Figure 7). Evidence for ISWs can be seen as high-frequency oscillations in results from autocovariance analyses (see Methods section) for 11 and 20 m salinity, temperature, and current velocity data at the midshelf mooring (Figure 7; salinity data shown). The ISWs had periods of 2–8 minutes, with a peak at ~3 minutes (Figure 7d), every 12.42 hours (semidiurnal tidal period). Large-amplitude ISWs on continental shelves have been observed previously [e.g., *Sandstrom et al.*, 1989; *Duda and Farmer*, 1999; *Chang and Dickey*, 2001; *Colosi et al.*, 2001]. The interaction of tides with the continental shelf edge during periods of stratification often leads to the formation of internal tides. These internal tides frequently result in nonlinear, high-energy bursts, or ISWs. The ISWs are important because they have the ability to bring nutrients and phytoplankton into or out of the euphotic layer, create turbulence and patchiness through mixing, and resuspend sediment from the ocean bottom [e.g., *Weidemann et al.*, 1996; *Bogucki et al.*, 1997; *Wang et al.*, 2001]. ISWs were not observed at the nearshore node, probably due to dissipation and reflection of the waves before reaching the shallower waters. Detailed analyses of ISWs observed at the HyCODE site are beyond the scope of this paper.

3.6. Water Mass/Turbidity Front

[24] Cross-shelf ship transect data indicate that a strong gradient in hydrographic properties and chlorophyll fluorescence was found between 8 and 15 km offshore of the

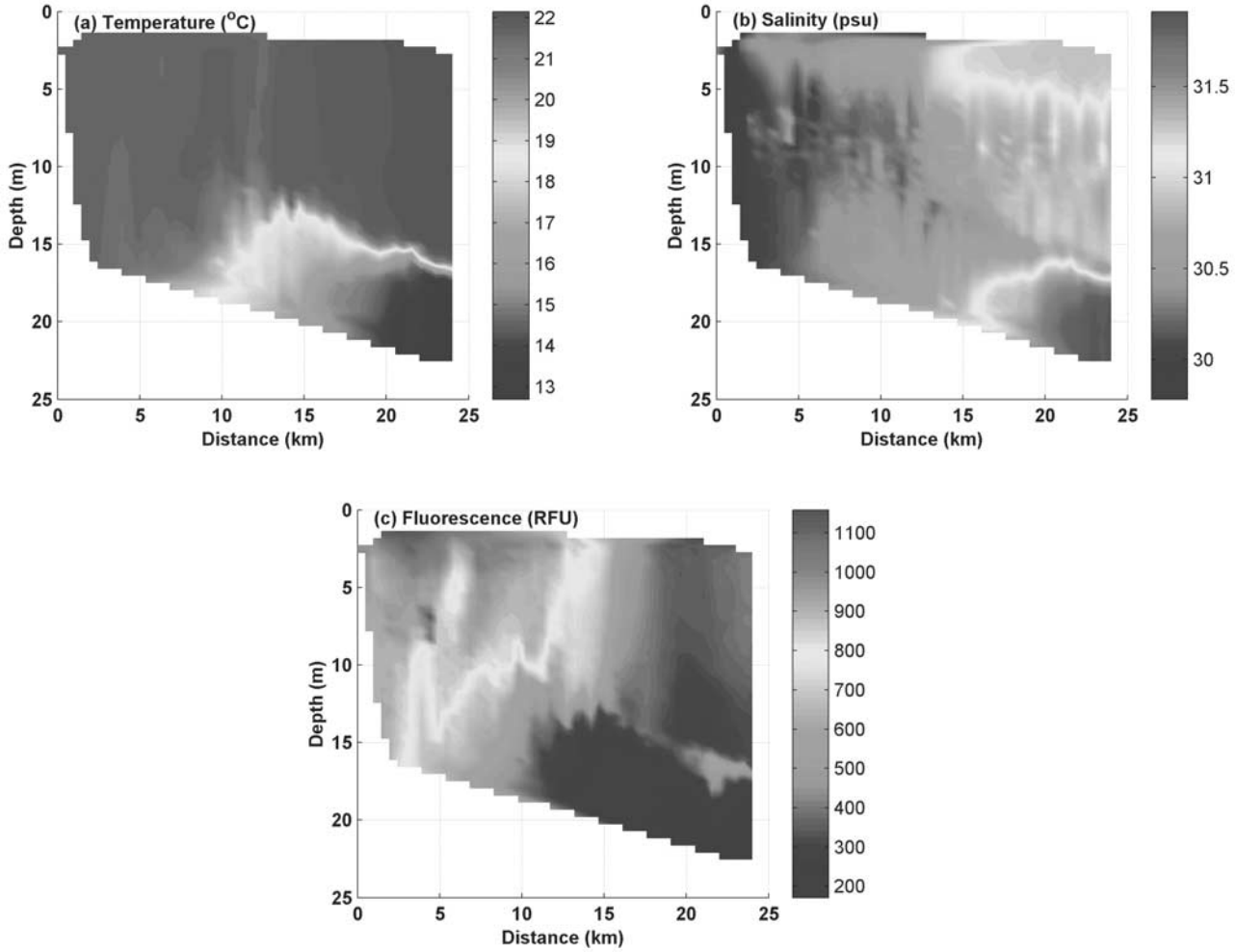

Figure 8. Cross-shelf transects of (a) temperature, (b) salinity, and (c) fluorescence data collected on July 27, 2000, illustrating the location of the water mass/turbidity front. See color version of this figure at back of this issue.

mouth of Great Bay (Figure 8; July 27 shown). A set of Ocean Portable Hyperspectral Imager for Low-Light Spectroscopy (Ocean PHILLS) [*Davis et al.*, 1999] images (RGB; not shown) from July 22 and July 27, 2000, also shows the presence of the water mass/turbidity front. This distinct and persistent front separated lower-salinity, higher-turbidity nearshore waters from higher-salinity, lower-turbidity offshore waters.

[25] Frontal turbidity differences were investigated by use of midshelf mooring and nearshore node optical and biological data. Profiled gelbstoff and total minus water absorption data at the midshelf location reveal that particles accounted for roughly 50% of absorbing materials (by difference) at all depths ($a_p(440) = 0.5*a_{t-w}(440)$, and $a_g(440) = 0.5*a_{t-w}(440)$; Figure 9). Results from chlorophyll *a* versus beam c scatterplot analyses indicate that phytoplankton dominated particulate matter at all depths (Figure 9). There is further evidence in $b_b(442)/b(440)$ versus [Chl *a*]/beam c plots, which reveal that the refractive index of particles at the near surface were associated with phytoplankton [*Twardowski et al.*, 2001] (Figure 9). Therefore, dissolved matter and phytoplankton dominated absorbing materials at the midshelf location. At the nearshore location, particulate absorption, compared to gelbstoff absorption, dominated the total minus water absorption signal ($a_p(440)/a_{t-w}(440) \approx 70\%$, $a_g(440)/a_{t-w}(440) \approx 30\%$) at all depths (Figure 9). Scatterplot results show that nearshore surface and intermediate waters were dominated by phytoplankton, whereas optical properties near the bottom were influenced by detrital material, likely due to sediment resuspension (Figure 9). Dissolved matter at the nearshore node was not as important to optical signals as it was at the midshelf mooring (particulate absorption signals dominated).

[26] Correlations and coherence with phase analyses (see Methods section) using chlorophyll fluorescence, absorption, and attenuation data were examined to determine the optical and biological properties that influenced the variability of turbidity. The temporal variability of chlorophyll fluorescence did not match that of absorption (440 nm) or attenuation (650 nm) at any depth at the nearshore node (Figure 5). This suggests that detritus likely controlled the variability of turbidity at the nearshore node. The temporal variability of chlorophyll *a* at 5 and 11 m at the midshelf location agreed well with that of absorption and attenuation at the same depths (Figure 5). Coherence of midshelf chlorophyll *a* with $a_{t-w}(440)$ and with c(650) was signifi-

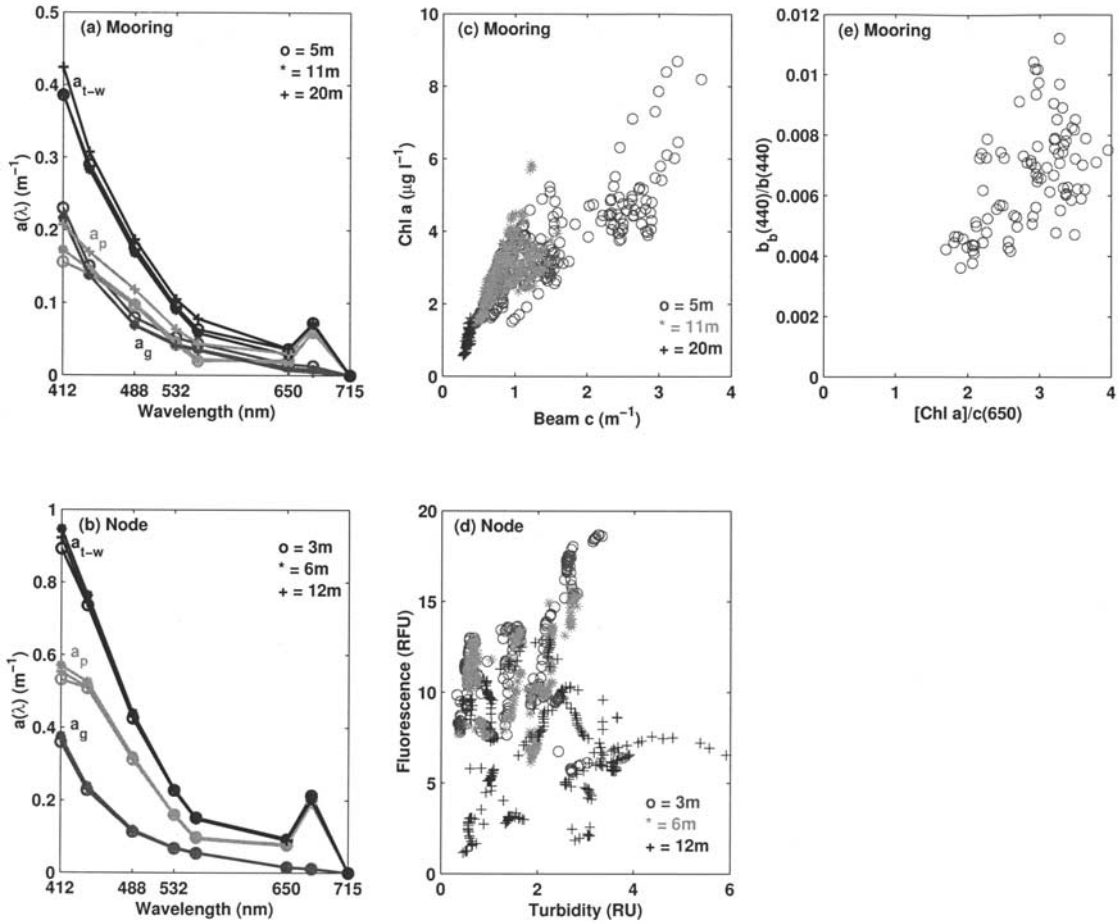

Figure 9. Total minus water, gelbstoff, and particulate absorption spectra collected from Slowdrop near the (a) midshelf mooring on July 26 and (b) nearshore node on July 25; scatterplots of (c) chlorophyll *a* versus beam c (660 nm) at 5 (circles), 11 (triangles), and 20 m (crosses) at the midshelf mooring; (d) chlorophyll fluorescence versus optical backscattering (measure of turbidity) at 3 (circles), 6 (triangles), and 12 m (crosses) at the nearshore node; and (e) backscattering to total scattering ratio at 440 nm ($b_b(442)/b(440)$) versus chlorophyll *a* to beam c (660 nm) ratio (chl *a*/beam c) at 5 m at the midshelf mooring.

cant (0° phase; Figure 10; a(440) coherence shown). Coherence was higher at the 11 m depth, closer to the chlorophyll *a* maximum. Therefore, this implies that phytoplankton controlled the variability of turbidity at the midshelf location. However, this was not the case for the entire deployment. During the period of May 24 to June 13, 2000, temporal variability in absorption spectra did not correlate well with variability of chlorophyll *a*, spectral attenuation, or scattering (data not shown). Preliminary analyses have shown that the spectral absorption signal near the surface agreed well with fast, southward moving, high-temperature, low-salinity water masses that moved past the HyCODE midshelf mooring location. This implies that colored dissolved organic matter (CDOM), possibly from the Hudson River outflow, dominated the optical signal in late spring.

3.7. Spatial Patchiness

[27] Cross-shelf shipboard transect data and complementary CODAR surface current data show that in addition to the persistent water mass/turbidity front, interactions of tidal currents with mean currents and the water mass/turbidity front led to the formation of small-scale convergence and divergence zones (on the order of a few kilometers) on the NYB inner continental shelf (Figure 11) (M. A. Moline et al., manuscript in preparation, 2002). The convergence and divergence zones coupled with the presence of a horizontal gradient of particulate matter from nearshore (higher) to midshelf (lower), formed small-scale patches of particles. Horizontal scales of patchiness were quantified using autocovariance analyses of cross-shelf transect data within the MLD (see Methods). Spatial scales of decorrelations for salinity and density were relatively consistent (∼7 km) between July 21 and July 31, 2000, except on July 24 when decorrelation scales dropped to ∼3 km. Spatial lags were more variable for temperature and chlorophyll fluorescence, which ranged between 3 and 9 km (Figure 11; salinity and chlorophyll fluorescence autocovariance for five transects shown). Because of the tidally influenced small-scale convergence and divergence zones observed in CODAR data, it was expected that spatial decorrelation scales would be more variable. However, most ship transects were made between 1230 and 1600 GMT, which may explain the

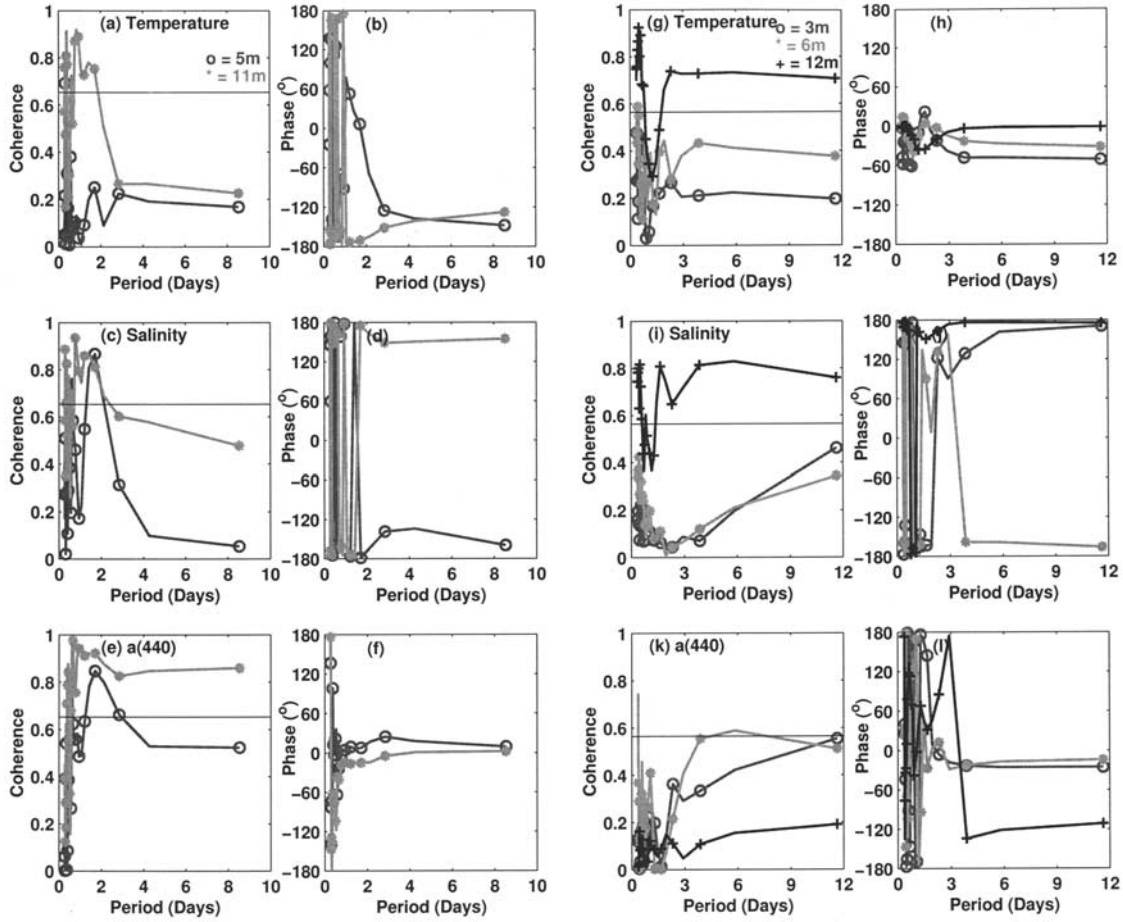

Figure 10. Coherence and phase analyses for (a) and (b) temperature, (c) and (d) salinity, and (e) and (f) total minus water absorption at 440 nm at 5 and 11 m at the midshelf mooring; and (g) and (h) temperature, (i) and (j) salinity, and (k) and (l) attenuation at 650 nm at 3, 6, and 12 m at the nearshore node. The black horizontal lines indicate statistical significance, calculated according to *Thompson* [1979].

relatively low variability of spatial decorrelation scales with time seen in the autocovariance analyses (i.e., the ship transects may have been temporally aliased).

[28] The more turbid waters nearshore contributed to shorter timescales of decorrelation for optical and biological parameters as compared to midshelf decorrelation scales, as seen in the results from autocovariance analyses (2–3 days at midshelf compared to 1 day nearshore; data not shown; see Methods). Timescales of decorrelation for hydrographic properties nearshore were comparable to those at midshelf, with temporal lags of 2–3 days (data not shown). The shorter optical and biological as compare to hydrographic decorrelation scales at the nearshore node was likely due to physical controls, e.g., advection by the coastal jet (discussed below). Coherence between chlorophyll fluorescence and salinity, temperature, and density for cross-shelf ship transect data was significant in the mixed layer on limited spatial scales (~5km), i.e., small-scale patchiness existed (data not shown).

3.8. Coastal Jet

[29] A mass of relatively cold, high-salinity, low-particulate water between 8 m and the ocean bottom (Figure 4d), accompanied by relatively fast southward moving currents (~30 cm s^{-1}; hereby referred to as the coastal jet; Figure 12) was observed at the nearshore node between July 22 and July 25, 2000. This jet extended approximately 5–10 km offshore, which scales with the Rossby radius of deformation. The Rossby radius of deformation is important to alongshore currents, as comparisons between the fluctuating Coriolis acceleration and the cross shelf pressure gradient indicate that the alongshore flows are primarily in geostrophic balance (R. J. Chant et al., manuscript in preparation, 2002). The chlorophyll fluorescence versus turbidity (optical backscatter) scatterplot at the node during the period of the jet indicates that particles carried by the jet were generally detritus. Chlorophyll fluorescence was significantly coherent with temperature (0° phase), salinity (180° phase), and density (180° phase) below the MLD when the coastal jet was observed (Figure 10). This suggests that the coastal jet greatly affected optical and biological variability at the node.

[30] At the midshelf mooring, we believe that the coastal jet also influenced physical, hydrographic, optical and biological variability. The coastal jet is associated with a shift from barotropic to baroclinic tidal flow on July 22 (data not

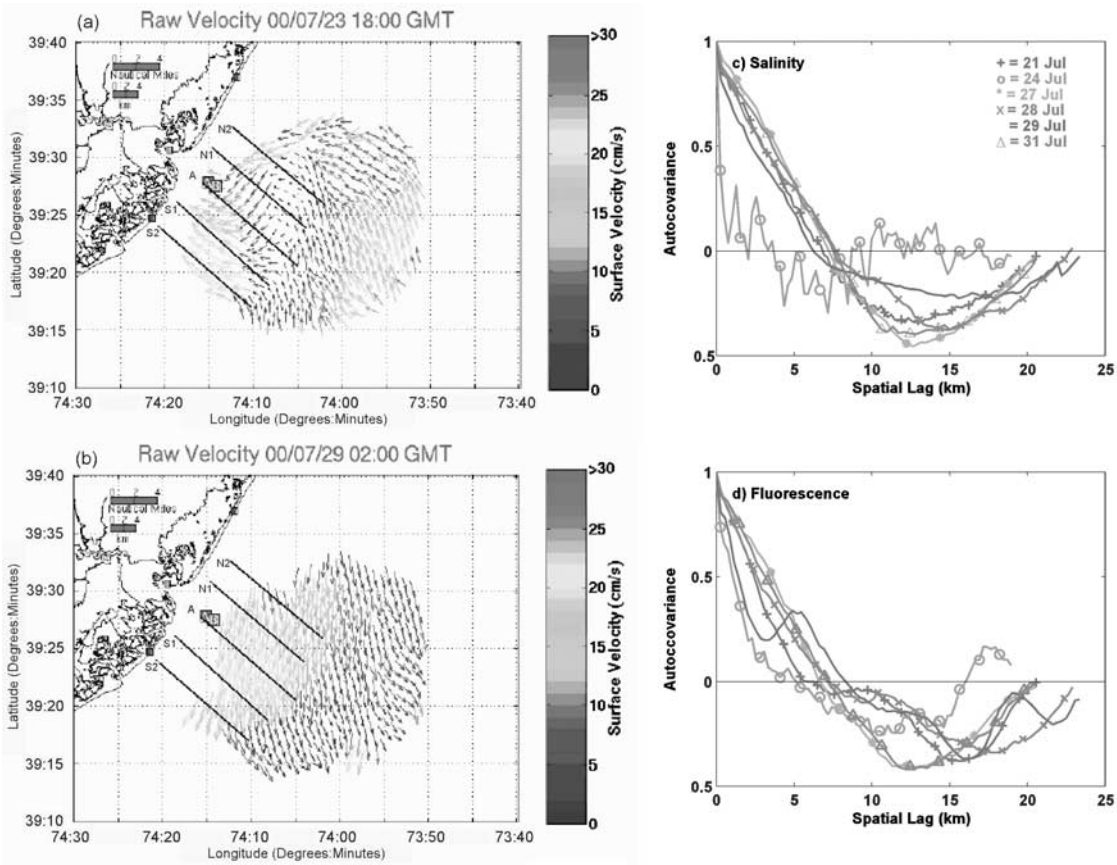

Figure 11. Surface currents derived from CODAR data (length of arrows are arbitrary, current velocities are represented by the color scale bar) for (a) July 23, 2000, at 1800 GMT when the tidal currents interacted with the nearshore jet to form small-scale convergence and divergence zones and (b) July 29, 2000, at 0200 GMT when tidal currents were flowing in the same direction as the mean currents, thus, spatial scales of decorrelation were much longer. Autocovariance analysis for (c) salinity and (d) chlorophyll fluorescence for 6 days of shipboard sampling. Note that most transect data were collected between 1230 and 1600 GMT, which may explain the relatively low variability of spatial decorrelation with time. See color version of this figure at back if this issue.

shown) and as the shoaling of the MLD from a depth of 14 to 8 m between July 22 and July 25 (Figure 4b). A large increase in chlorophyll *a*, absorption, and attenuation at 5 m at the midshelf mooring occurred in the same time period (Figure 5). The chlorophyll *a* versus beam c scatterplot reveals that phytoplankton dominated the midshelf water column during the period of the coastal jet. We hypothesize that this increase in biomass (inferred from chlorophyll *a*) was due to the displacement of lower-salinity, higher-nutrient, or higher-biomass nearshore waters to the midshelf region by the coastal jet. We attribute this apparent "bloom" to advection of higher-biomass waters, not localized growth. Increases in optical and biological properties at the midshelf mooring occurred at the same time as changes in hydrographic properties at the nearshore node. A nutrient-induced bloom would have resulted in a 3–5 day time lag between changes in hydrographic, optical, and biological properties. We also suggest that the chlorophyll maximum at midshelf shoaled from a depth of 16 to ~10 m because of the coastal jet. This is evidenced in the high coherence (180° phase) and significant inverse correlation between hydrographic properties and chlorophyll *a* within the MLD during the time period of the coastal jet (Figure 10). Also, currents below ~8 m flowed offshore during the time period of the coastal jet.

[31] It is hypothesized that the coastal jet originated from an upwelling center approximately 30 km north of Great Bay, NJ (~39.36°N, 74.15°W; meteorological, physical, hydrographic, optical and biological data were collected during the summer 2000 COJET experiment; D. Johnson, pers. comm.). This is evidenced in hydrographic measurements; the T-S signature of the upwelled water at the COJET site was the same as that found at 12 m depth at the nearshore node (Figure 13). Optical and biological data from COJET reveal that the upwelled water was low in chlorophyll fluorescence and particulates (inferred from scattering). The upwelling at the COJET site commenced on July 21, 2000, following 3 days of upwelling favorable winds. Current direction also shifted from northward to southward on July 21.

[32] It has been seen from past LEO-15 data sets, particularly the summer 1998 LEO-15 field experiment, that the coastal jet, in combination with local upwelling fronts, carried with it high-particulate, high-chlorophyll

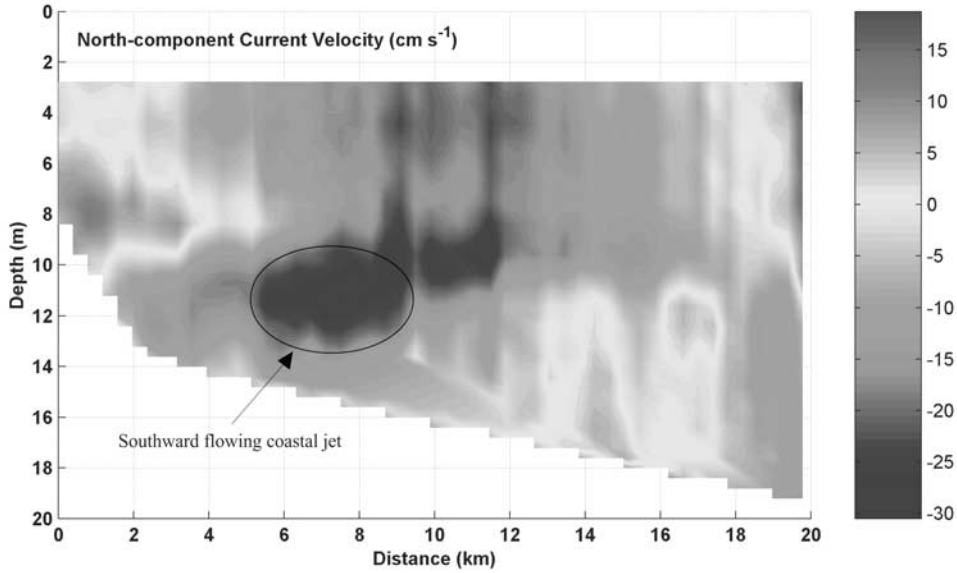

Figure 12. Cross-shelf transect of north component current velocity data from the towed ADCP collected on July 24, 2000. See color version of this figure at back of this issue.

fluorescence water, eventually replacing all shelf waters (to the continental slope) with turbid water (see http://marine.rutgers.edu/cool/). Local, strong, southerly winds were responsible for offshore movement of newly formed upwelling fronts. After the local upwelling favorable winds relaxed to light and variable winds for several days, the upwelling center with an embedded cyclonic eddy grew rapidly and continued to move offshore, eventually dissipating at the shelf break. This is different from what we observed during the summer 2000 HyCODE field experiment, when the coastal jet originated from a remote upwelling center and nearshore water was replaced with low-particulate, low-chlorophyll fluorescence water advected by the coastal jet. However, effects of the coastal jet at the midshelf location were the same, as relatively clear water was replaced with high-particulate, high-biomass water.

4. Toward the Future

[33] The shallow waters and close proximity to freshwater flows (Hudson River, Great Bay, etc.) and the coastal jet result in relatively short temporal and spatial scales of variability in physical, hydrographic, optical, and biological parameters, increasing from nearshore toward the midshelf. High-frequency variability in physical, biological, and optical parameters due to turbulence and ISWs are commonly observed in coastal regions. In shallow regions like the HyCODE site, coastal processes (e.g., tides, internal waves, upwelling, coastal jets, eddies, river and estuarine outflows, etc.) have the potential to interact with each other as well as with shelf/slope frontal processes (e.g., eddies, filaments, jets, meanders, etc.) to create dynamic small-scale convergence and divergence zones, affecting the biology, particulates, and optical properties of the water column. Water mass movements are more important to biological variability in shallow waters, whereas biological controls (e.g., zooplankton grazing) impact biological variability in open ocean regions such as the Arabian Sea [*Lee et al.*, 2000]. *Washburn et al.* [1998] found spatial decorrelation scales of tens of km for various properties in the open ocean, whereas spatial decorrelation scales are on the order of a few km at the HyCODE site.

[34] As an increasing number of coastal ocean field experiments shift from the shelf break toward the coast, sampling schemes must be adjusted to account for the more dynamic and complex physical processes, shorter temporal and spatial decorrelation scales, and more productive and turbid nearshore waters [see *Dickey*, 1991, Figure 1, 2002].

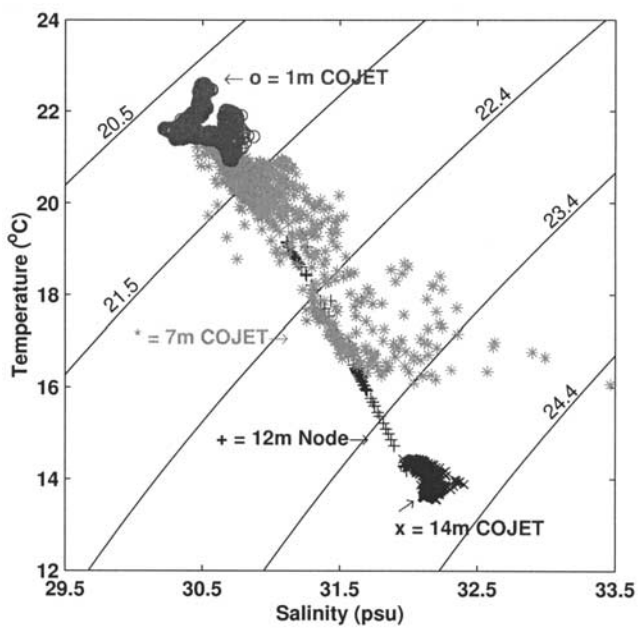

Figure 13. Temperature versus salinity (T-S) data from 12 m depth at the nearshore node (pluses), and 1 m (circles), 7 m (triangles), and 14 m (crosses) depth at the COJET experimental region between July 22 and July 25, 2000.

Satellite images coupled with real-time in-water data and forecast models provide a means for adaptive sampling [e.g., *Dickey*, 2002; M. A. Moline et al., manuscript in preparation, 2002]. Hyperspectral ocean color images and medium- to long-range CODAR surface currents supply a synoptic view of processes with horizontal scales of tens of meters to tens of kilometers. High temporal frequency (sampling rate of 1 min or less) physical, hydrographic, optical, chemical, and biological moored and moored profiling (node) instrumentation at several locations (midshelf and nearshore, or upstream and downstream of mean circulation, or both) is necessary for resolving tides, internal solitary and surface waves, turbulence, sediment resuspension, MLD dynamics, deep water mass movements (e.g., coastal jets) changes in nutrients, phytoplankton light adaptation, etc. (see reviews by *Dickey* [1991, 2002]). The use of towed, profiling packages (undulating), AUVs, floats, and/or gliders across the shelf provides high spatial resolution (vertical and horizontal) data for studies of advection, upwelling, river and estuarine flows, frontal dynamics, and water mass intrusions (e.g., filaments, meanders, and eddies) and their effects on water column biological and optical properties. The data collected will likely be utilized with nested sampling grids and data assimilation models to provide information and predictions of an unprecedented number of interdisciplinary variables on time and space scales spanning on order of 6 to 7 orders of magnitude.

[35] The continuing study of the relationships between physical processes and bio-optical properties in nearshore coastal regions is important for establishing an understanding of particulate (including organisms, sediments, contaminants, etc.) as well as dissolved matter movement and distribution in the water column and near the ocean floor in areas most impacted and utilized by humans. Knowledge of particle and dissolved matter characteristics close to shore is necessary for: 1) studies of anthropogenic effects on the coastal ocean, 2) the development of interdisciplinary models to predict the movement and distribution of biology, and 3) the development and testing of ocean color algorithms to derive organic matter and primary production from remotely sensed data, which is important for quantifying the global carbon budget, particularly in nearshore coastal regions.

[36] We have gained valuable insight into nearshore coastal processes and their effects on biology as well as for the design of future nearshore interdisciplinary coastal programs [e.g., *Glenn et al.*, 2000; *Dickey*, 2002]. Our results will enable interpretation of data obtained during complementary experiments and also allow us to build on the current HyCODE project. For example, knowledge of frontal characteristics will facilitate analyses of temporal and spatial variability of remote sensing reflectance spectral shapes and thus, algorithm development. Information on particle patch size is necessary for the design of new remote sensing instrumentation for coastal sites with respect to pixel size and swath width. Last, our identification of various temporal and spatial scales of coastal processes will aid in the determination of instrument type, placement, and sampling rates as well as model time steps and grid spacing for future oceanographic programs.

[37] **Acknowledgments.** This work was supported by the Office of Naval Research Environmental Optics Program as part of the HyCODE program. We would also like to thank Curt Davis and Bill Snyder for Ocean PHILLS RGB images; Don Johnson for complementary COJET data; Josh Kohut for the CODAR data; Bob Chant for the valuable discussions; François Baratange, Mike Crowley, John Fracassi, Xuri Yu, and especially Songnian Jiang for their help in data processing; Derek Manov, David Sigurdson, and Frank Spada for their engineering support; Kristie Andresen, Trisha Bergmann, Amanda Briggs, Liz Creed, Erika Heine, Christy Herren, Matt Oliver, Christina Orrico, and Hank Statscewich for their help in data collection; Rose Petrecca, Bobbie Zlotnik, and the rest of the staff at Rutgers University Marine Field Station (RUMFS); and the ship captains and crews of the R/V *Caleta*, R/V *Endeavor*, R/V *Northstar*, and R/V *Walford*.

References

Abbott, M. R., and R. M. Letelier, Decorrelation scales of chlorophyll as observed from bio-optical drifters in the California Current, *Deep Sea Res., Part II*, *45*, 1639–1667, 1998.

Abbott, M. R., K. H. Brink, C. R. Booth, D. Blasco, M. S. Swenson, C. O. Davis, and L. A. Condispoti, Scales of variability of bio-optical properties as observed from near-surface drifters, *J. Geophys. Res.*, *100*, 13,345–13,367, 1995.

Barth, J., P. M. Kosro, J. A. Austin, and S. D. Pierce, Three dimensional hydrographic and velocity fields over the Oregon shelf during time-dependent upwelling, *Eos Trans. AGU*, *80*(49), Ocean Sci. Meet. Suppl., OS31K-01, 1999.

Biscaye, P. E., Preface: Shelf Edge Exchange Processes in the southern Middle Atlantic Bight: SEEP-II, *Deep Sea Res. Part II*, *41*, 229–230, 1994.

Biscaye, P. E., R. F. Anderson, and B. L. Deck, Fluxes of particles and constituents to the eastern United States continental slope and rise: SEEP-I, *Cont. Shelf Res.*, *8*, 855–904, 1988.

Biscaye, P. E., C. N. Flagg, and P. G. Falkowski, The Shelf Edge Exchange Processes experiment, SEEP-II: An introduction to hypotheses, results, and conclusions, *Deep Sea Res., Part II*, *41*, 231–252, 1994.

Bogucki, D., T. Dickey, and L. G. Redekopp, Sediment resuspension and mixing by resonantly generated internal solitary waves, *J. Phys. Oceanogr.*, *27*, 1181–1196, 1997.

Boss, E., W. S. Pegau, M. Lee, M. Twardowski, M. Shibanov, E. Korotev, and F. Baratange, Measurements and application of the back-scattering ratio bbp/bp, paper presented at ASLO 2001 Aquatic Sciences Meeting, Am. Soc. of Limnol. and Oceanogr., Albuquerque, N. M., 2001.

Bourne, D. W., and C. S. Yentsch, Phytoplankton, primary production, and microbiology, in *Georges Bank*, edited by R. H. Backus, pp. 210–212, MIT Press, Cambridge, Mass., 1987.

Brooks, D. A., Physical oceanography of the shelf and slope seas from Cape Hatteras to Georges Bank: A brief overview, in *The Northeast Shelf Ecosystem*, edited by K. Sherman, N. A. Jaworski, and T. J. Smayda, pp. 47–74, Blackwell Sci., Malden, Mass., 1996.

Bumpus, D. F., A description of the circulation on the continental shelf of the east coast of the United States, *Progr. Oceanogr.*, *6*, 111–157, 1973.

Chang, G. C., Analyses of bio-optical variability related to physical processes on the southern New England continental shelf: July 1996–June 1997, Ph.D. diss., Univ. of Calif., Santa Barbara, 1999.

Chang, G. C., and T. D. Dickey, Optical and physical variability on time scales from minutes to the seasonal cycle on the New England shelf: July 1996 to June 1997, *J. Geophys. Res.*, *106*, 9435–9453, 2001.

Chang, G., S. Jiang, X. Yu, S. Zedler, D. Manov, D. Sigurdson, F. Spada, and T. Dickey, Data report: Hyperspectral Coastal Ocean Dynamics Experiment (HyCODE) Deployment II: 25 July–15 September 2000, *Ocean Phys. Lab. Tech. Rep. OPL-05-00*, 42 pp., Ocean Phys. Lab., Univ. of Calif. at Santa Barbara, Santa Barbara, 2000.

Chang, G. C., T. D. Dickey, and A. J. Williams III, Sediment resuspension on the Middle Atlantic Bight continental shelf during Hurricanes Edouard and Hortense: September 1996, *J. Geophys. Res.*, *106*, 9517–9531, 2001.

Chelton, D. B., A. W. Bratkovich, R. L. Bernstein, and P. M. Kosro, Poleward flow off central California during the spring and summer of 1981 and 1984, *J. Geophys. Res.*, *93*, 10,604–10,620, 1988.

Colosi, J. A., J. F. Lynch, R. Beardsley, G. Gawarkiewicz, A. Scotti, and C. S. Chiu, Observations of nonlinear internal waves on the outer New England continental shelf during the summer shelfbreak Primer study, *J. Geophys. Res.*, *106*, 9587–9602, 2001.

Davis, C. O., M. Kappus, J. Bowles, J. Fisher, J. Antoniades, and M. Carney, Calibration, characterization and first results with the Ocean PHILLS hyperspectral imager, paper presented at SPIE Conference on Imaging Spectrometry, V, Soc. of Photo-Opt. Instrum. Eng., Bellingham, Wash., 1999.

Dickey, T. D., The emergence of concurrent high-resolution physical and bio-optical measurements in the upper ocean and their applications, *Rev. Geophys.*, *29*, 383–413, 1991.

Dickey, T., A vision of oceanographic instrumentation and technologies in the early 21st century, in *Oceans 2020: Science for Future Needs*, edited by J. G. Field, G. Hempel, and C. P. Summerhayes, Island Press, Washington D. C., 213–256, 2002.

Dickey, T. D., and A. J. Williams III, Physical processes and their effects on optical and acoustical variability on the New England shelf, *J. Geophys. Res.*, *106*, 9427–9434, 2001.

Dickey, T. D., J. Marra, T. Granata, C. Langdon, M. Hamilton, J. Wiggert, D. Siegel, and A. Bratkovich, Concurrent high resolution bio-optical and physical time series observations in the Sargasso Sea during the spring of 1987, *J. Geophys. Res.*, *96*, 8463–8663, 1991.

Dickey, T. D., T. Granata, J. Marra, C. Langdon, J. Wiggert, Z. Chai-Jochner, M. Hamilton, J. Vazquez, M. Stramska, R. Bidigare, and D. Siegel, Seasonal variability of bio-optical and physical properties in the Sargasso Sea, *J. Geophys. Res.*, *98*, 865–898, 1993.

Dickey, T. D., J. Marra, M. Stramska, C. Langdon, T. Granata, A. Plueddemann, R. Weller, and J. Yoder, Bio-optical and physical variability in the subarctic North Atlantic Ocean during the spring of 1989, *J. Geophys. Res.*, *99*, 22,541–22,556, 1994.

Dickey, T., et al., Initial results from the Bermuda Testbed Mooring program, *Deep Sea Res., Part I*, *45*, 771–794, 1998a.

Dickey, T., J. Marra, D. E. Sigurdson, R. A. Weller, C. S. Kinkade, S. E. Zedler, J. D. Wiggert, and C. Langdon, Seasonal variability of bio-optical and physical properties in the Arabian Sea: October 1994–October 1995, *Deep Sea Res., Part II*, *45*, 2001–2025, 1998b.

Dickey, T., S. Jiang, X. Yu, S. Zedler, D. Manov, D. Sigurdson, F. Spada, and G. Chang, Data report: Hyperspectral Coastal Ocean Dynamics Experiment (HyCODE) Deployment I: 16 May–25 July 2000, *Ocean Phys Lab Tech. Rep. OPL-04-00*, 42 pp., Univ. of Calif. at Santa Barbara, 2000.

Dickey, T., et al., Physical and biogeochemical variability from hours to years at the Bermuda Testbed Mooring site: June 1994–March 1998, *Deep Sea Res., Part II*, *48*, 2105–2140, 2001.

Duda, T. F., and D. M. Farmer (Eds.), The 1998 WHOI/IOS/ONR Internal Solitary Wave Workshop: Contributed Papers, *Tech. Rep. WHOI-99-07*, 247 pp., Woods Hole Oceanogr. Inst., Woods Hole, Mass., 1999.

Flagg, C. N., C. D. Wirick, and S. L. Smith, The interaction of phytoplankton, zooplankton and currents from 15 months of continuous data in the Mid-Atlantic Bight, *Deep Sea Res., Part II*, *41*, 411–435, 1994.

Glenn, S. M., T. D. Dickey, B. Parker, and W. Boicourt, Long-term real-time coastal ocean observation networks, *Oceanography*, *13*, 24–34, 2000.

Hamilton, M., T. C. Granata, T. D. Dickey, J. D. Wiggert, D. A. Siegel, J. Marra, and C. Langdon, Diel variations of bio-optical properties in the Sargasso Sea, *SPIE Soc. Opt. Eng.*, *X*, 214–224, 1990.

Kemp, P. F., Microbial carbon utilization on the continental shelf and slope during the SEEP-II experiment, *Deep Sea Res., Part II*, *41*, 563–581, 1994.

Lee, C. M., B. H. Jones, K. H. Brink, and A. S. Fischer, The upper-ocean response to monsoonal forcing in the Arabian Sea: Seasonal and spatial variability, *Deep Sea Res., Part II*, *47*, 1177–1226, 2000.

Maffione, R. A., and D. R. Dana, Instruments and methods for measuring the backward-scattering coefficient of ocean waters, *Appl. Opt.*, *36*, 6057–6067, 1997.

Mann, K. H., and J. R. N. Lazier, *Dynamics of Marine Ecosystems*, 466 pp., Blackwell Sci., Cambridge, Mass., 1991.

Mayer, D. A., The structure of circulation: MESA physical oceanographic studies in New York Bight, 2, *J. Geophys. Res.*, *87*, 9579–9588, 1982.

Mountain, D. G., The volume of shelf water in the Middle Atlantic Bight: Seasonal and interannual variability, 1977–1987, *Cont. Shelf Res.*, *11*, 251–267, 1991.

Pickart, R. S., D. J. Torres, T. J. McKee, M. J. Caruso, and J. E. Przystup, Diagnosing a meander of the shelf break current in the Middle Atlantic Bight, *J. Geophys. Res.*, *104*, 3121–3132, 1999.

Sandstrom, H., J. A. Elliot, and N. A. Cochrane, Observing groups of solitary internal waves and turbulence with BATFISH and echo-sounder, *J. Phys. Oceanogr.*, *19*, 987–997, 1989.

Sherman, K., M. Grosslein, D. Mountain, D. Busch, J. O'Reilly, and R. Theroux, The northeast shelf ecosystem: An initial perspective, in *The Northeast Shelf Ecosystem*, edited by K. Sherman, N. A. Jaworski, and T. J. Samayda, pp. 103–126, Blackwell Sci., Cambridge, Mass., 1996.

Stramska, M., and T. D. Dickey, Short-term variations of the bio-optical properties of the ocean in response to cloud-induced irradiance fluctuations, *J. Geophys. Res.*, *97*, 5713–5721, 1992.

Stramska, M., and T. D. Dickey, Short-term variability of the underwater light field in the oligotrophic ocean in response to surface waves and clouds, *Deep Sea Res., Part I*, *45*, 1393–1410, 1998.

Thompson, R. O. R. Y., Coherence significance levels, *J. Atmos. Sci.*, *36*, 2020–2021, 1979.

Trowbridge, J. H., and A. R. M. Nowell, An introduction to the Sediment Transport Events on Shelves and Slopes (STRESS) program, *Cont. Shelf Res.*, *14*, 1057–1061, 1994.

Twardowski, M. S., E. Boss, J. B. Macdonald, W. S. Pegau, A. H. Barnard, and J. R. V. Zaneveld, A model for estimating bulk refractive index from the optical backscattering ratio and the implications for understanding particle composition in case I and case II waters, *J. Geophys. Res.*, *106*, 14,129–14,142, 2001.

United Nations Educational, Scientific, and Cultural Organization (UNESCO), Background papers and supporting data on the international equation of state, *UNESCO Technical Papers in Marine Science*, *38*, 192 pp., Paris, France, 1981.

Wang, B. J., D. Bogucki, and L. G. Redekopp, Particle motions and distributions resulting from the action of solitary waves, *J. Geophys. Res.*, *106*, 9565–9586, 2001.

Washburn, L., B. M. Emery, B. H. Jones, and D. G. Ondercin, Eddy stirring and phytoplankton patchiness in the subarctic North Atlantic in late summer, *Deep Sea Res., Part I*, *45*, 1411–1439, 1998.

Weidemann, A. D., W. S. Pegau, L. A. Jugan, and T. E. Bowers, Tidal influences on optical variability in shallow water, *SPIE Proceedings from Ocean Optics XIII*, edited by S. G. Ackleson and R. Frouin, pp. 320–325, Soc. of Photo-Opt. Intrum. Eng., Bellingham, Wash., 1996.

Wollast, R., Evaluation and comparison of the global carbon cycle in the coastal zone and in the open ocean, in *The Sea*, vol. 10, *The Global Coastal Ocean*, edited by K. H. Brink and A. R. Robinson, vol. 10, pp. 213–252, J. Wiley, New York, 1998.

Wu, Y., L. Washburn, and B. H. Jones, Buoyant plume dispersion in a coastal environment: Evolving plume structure and dynamics, *Cont. Shelf Res.*, *14*, 1001–1023, 1994.

G. C. Chang and T. D. Dickey, Ocean Physics Laboratory, University of California at Santa Barbara, 6487 Calle Real Unit A, Santa Barbara, CA 93117, USA. (grace.chang@opl.ucsb.edu)

S. M. Glenn and O. M. Schofield, Institute of Marine and Coastal Sciences, Rutgers University, 71 Dudley Road, New Brunswick, NJ 08901–8521, USA.

M. A. Moline, Biological Sciences Department, California Polytechnic State University, San Luis Obispo, CA 93407, USA.

W. S. Pegau, College of Oceanic and Atmospheric Sciences, Oregon State University, Corvallis, OR 97331, USA.

A. D. Weidemann, Naval Research Laboratory, Code 7333, Building 1009, Stennis Space Center, MS 39529–5004, USA.

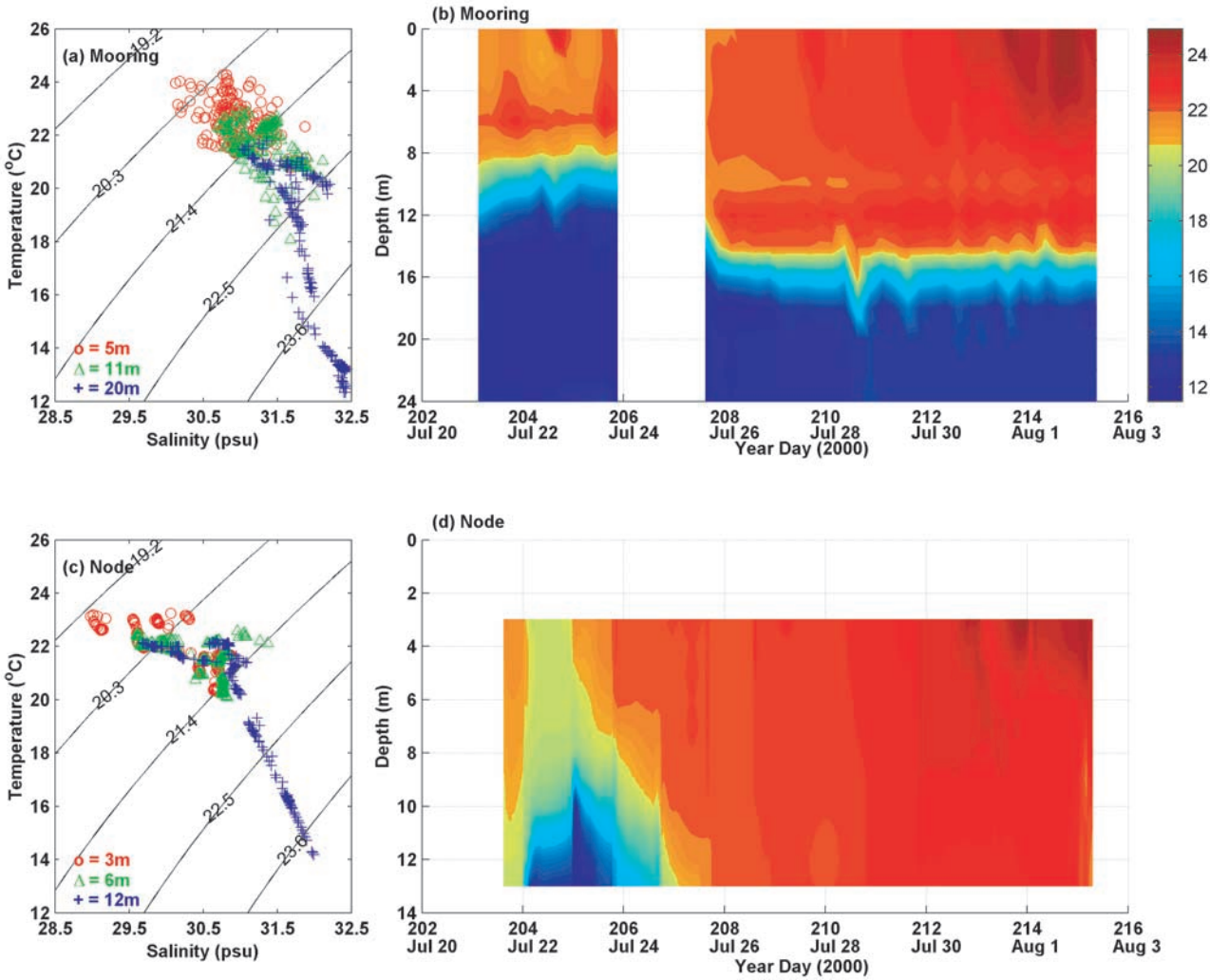

Figure 4. (a) The 4 hour averaged temperature versus salinity (T-S) data, and (b) the time series contour plot of the 4 hour averaged temperature from the midshelf mooring (the temporal gap is when mooring instruments were recovered and redeployed); (c) the 1 hour averaged temperature versus salinity data, and (d) the time series contour plot of the 1 hour averaged temperature from the nearshore profiling node. Density lines on T-S plots were calculated according to *United Nations Educational, Scientific, and Cultural Organization* (*UNESCO*) [1981] algorithms and are labeled. The color scale bar represents Figures 4b and 4d.

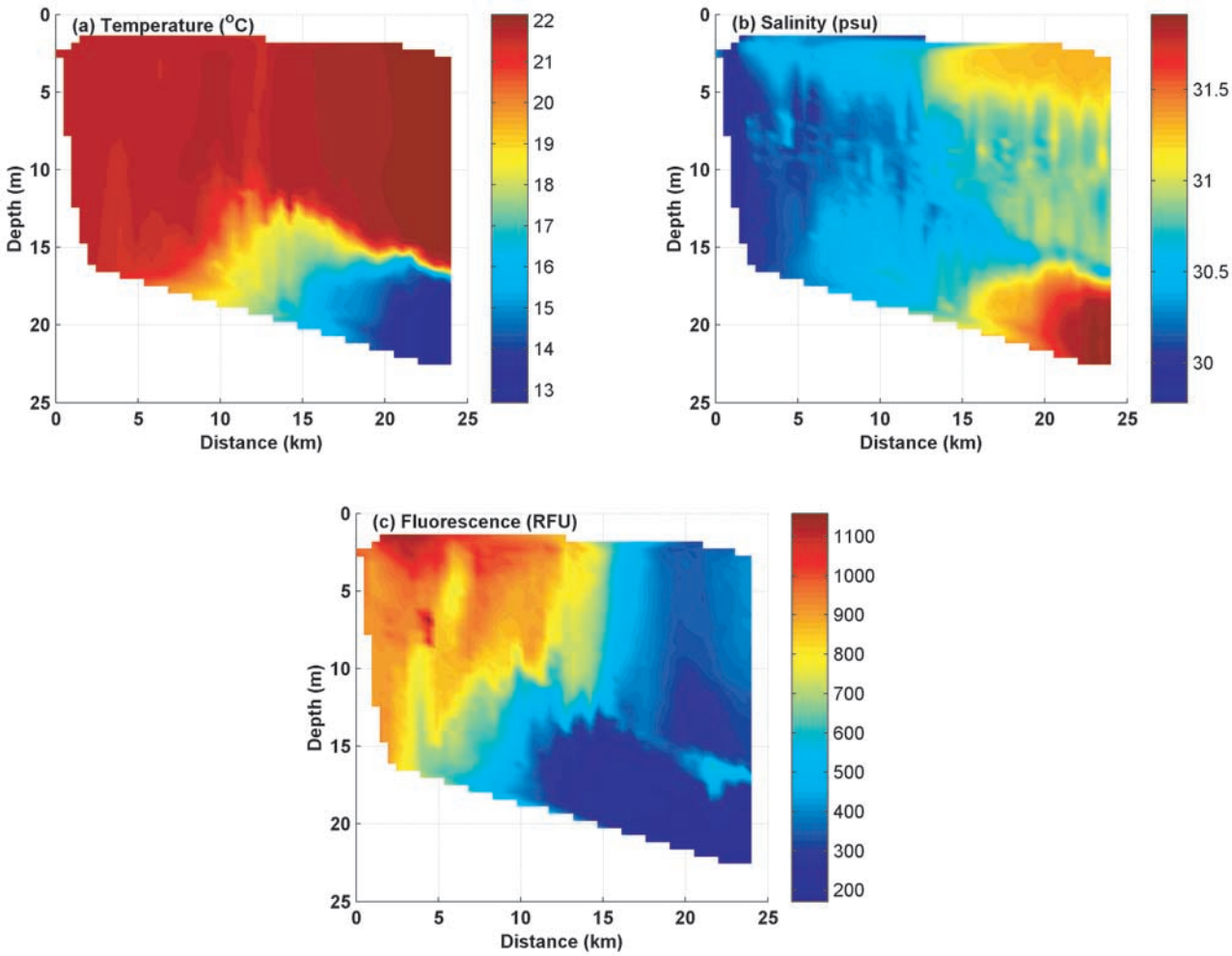

Figure 8. Cross-shelf transects of (a) temperature, (b) salinity, and (c) fluorescence data collected on July 27, 2000, illustrating the location of the water mass/turbidity front.

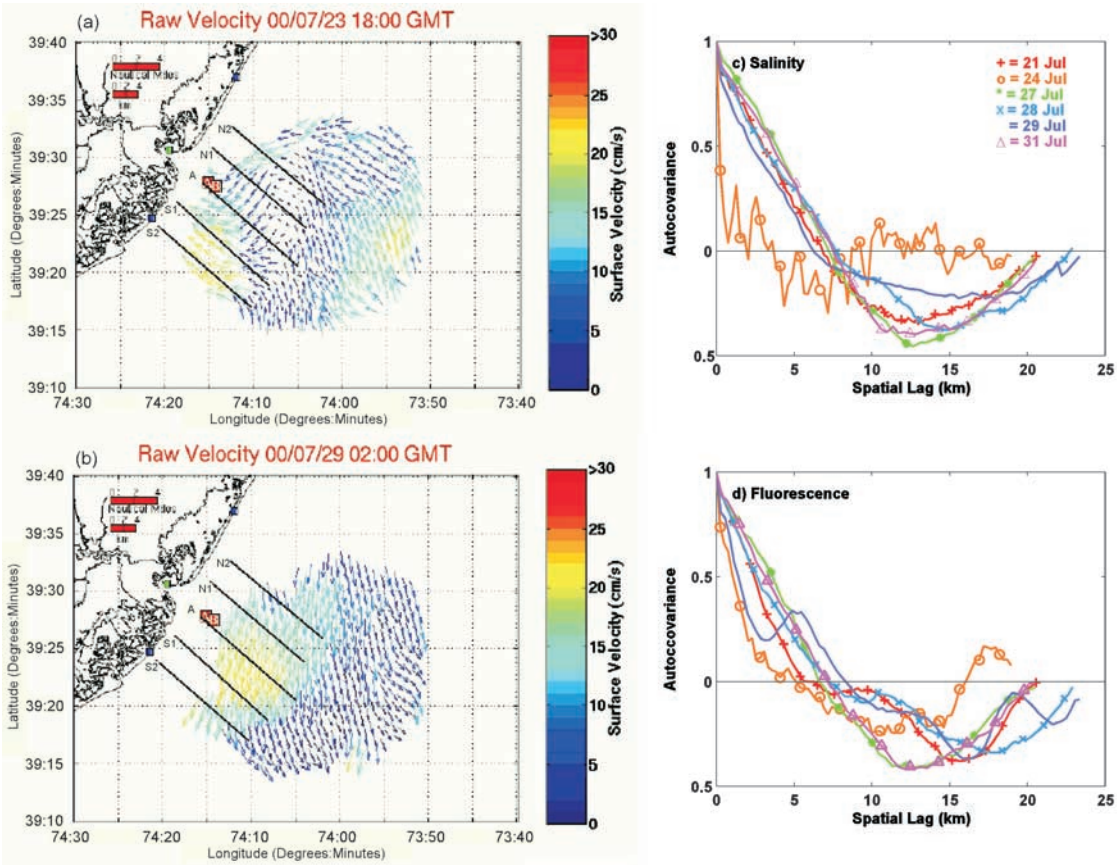

Figure 11. Surface currents derived from CODAR data (length of arrows are arbitrary, current velocities are represented by the color scale bar) for (a) July 23, 2000, at 1800 GMT when the tidal currents interacted with the nearshore jet to form small-scale convergence and divergence zones and (b) July 29, 2000, at 0200 GMT when tidal currents were flowing in the same direction as the mean currents, thus, spatial scales of decorrelation were much longer. Autocovariance analysis for (c) salinity and (d) chlorophyll fluorescence for 6 days of shipboard sampling. Note that most transect data were collected between 1230 and 1600 GMT, which may explain the relatively low variability of spatial decorrelation with time.

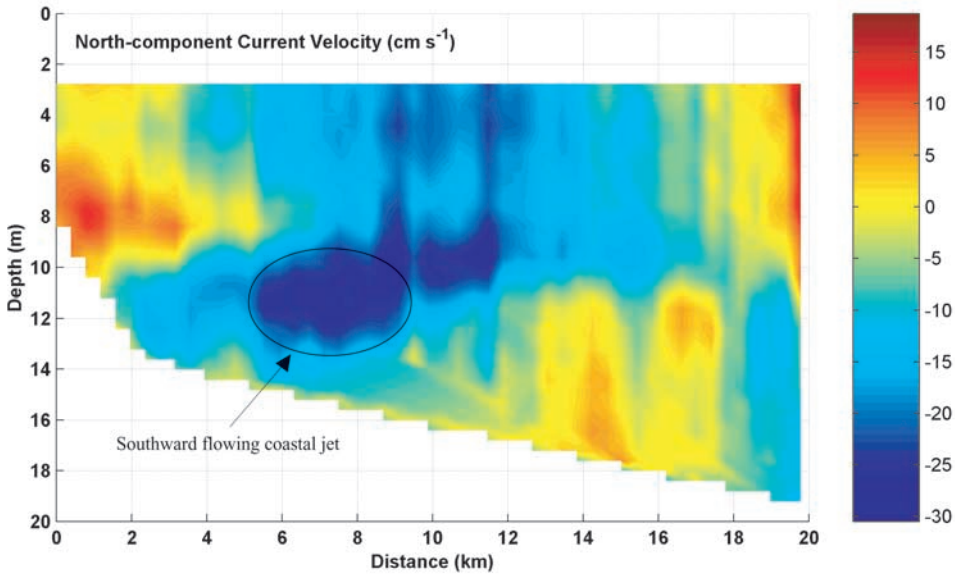

Figure 12. Cross-shelf transect of north component current velocity data from the towed ADCP collected on July 24, 2000.